Received 7 January 2024; revised 11 February 2024; accepted 24 February 2024. Date of publication 5 March 2024; date of current version 21 March 2024.

Digital Object Identifier 10.1109/OJCOMS.2024.3372881

Laser-Empowered UAVs for Aerial Data Aggregation in Passive IoT Networks

AMR M. ABDELHADY [1] (Member, IEEE), ABDULKADIR CELIK [1] (Senior Member, IEEE), CARLES DIAZ-VILOR [2] (Student Member, IEEE), HAMID JAFARKHANI [2] (Fellow, IEEE), AND AHMED M. ELTAWIL [1] (Senior Member, IEEE)

[1]Computer Electrical, and Mathematical Science and Engineering Division, King Abdullah University of Science and Technology, Thuwal 23955, Makkah, Saudi Arabia

[2]Center for Pervasive Communications and Computing, Department of Electrical Engineering and Computer Science, University of California at Irvine, Irvine, CA 92697, USA

CORRESPONDING AUTHOR: A. M. ABDELHADY (e-mail: amr.abdelhady@kaust.edu.sa)

This work was supported in part by NEOM under Grant 4849, and in part by the King Abdullah University of Science and Technology (KAUST) through the OFP2023 Program under Grant URF/1/5532-01-01.

ABSTRACT This paper investigates the maximization of data harvested by an uncrewed aerial vehicle (UAV) that supports Internet of Things (IoT) deployment scenarios. The novelty of the paper is that we study the feasibility of battery-free UAV and IoT device deployment where the UAV is powered by a ground laser source, and the IoT devices are powered by a power beacon via bistatic backscattering. We aim to optimize the UAV trajectory while minimizing the laser energy consumption throughout the entire flight by tuning the laser power and the power beacon radiated temporal power profiles. Upon considering an unspecified flying time, we adopt path discretization and resort to the single-block successive convex approximation (SCA) to solve the data collection maximization problem. In addition to considering the UAV dynamics and power budget, two novel SCA-compatible bounds are introduced for the product of positive mixed convex/concave functions. Finally, the simulation results show that the proposed algorithm increases the data collected under different operation conditions by approximately 90%.

INDEX TERMS Laser-powered UAVs, trajectory optimization, backscatter communications, resource allocation.

I. INTRODUCTION

ENERGY provisioning and management of airborne-aided IoT networks has garnered significant research interest due to the power-limited nature of both uncrewed aerial vehicles (UAVs) and Internet of Things (IoT) devices, as evidenced in [1], [2], [3], [4] and the references therein. Moreover, recent advances in acquisition, pointing, and tracking (APT) technologies have increased the affordability of ground-to-air laser links [5], [6]. Consequently, numerous recent works have emphasized laser-based UAV charging [7], [8], [9], [10], [11], [12] due to its (*i*) relatively high power transfer efficiency compared to other schemes, (*ii*) miniature transmission and reception apertures, and (*iii*) capability of supporting longer ranges and prolonged missions. In particular, different UAV charging technologies were compared to laser-based charging in [7], where simulations confirmed the superiority of laser charging. Additionally, PowerLight Technologies and Ericsson managed to power a 5G base station through safe laser beaming.[1]

Exploiting free space optical (FSO) links to provide airborne simultaneous lightwave information and power transfer (SLIPT) was introduced in [8], where the inherent energy-information transfer tradeoff was highlighted. In [13], the authors provided coverage analysis for large-scale deployments, which served as guidelines for the density of deployment of laser stations. In fact, operation optimization has taken a significant share of research contributions in this area [10], [11], [12], [14], [15], [16], [17], [18], [19], [20]. Among the aforementioned works, optimal UAV

[1]https://www.ericsson.com/en/news/2021/10/ericsson-and-powerlight-achieve-base-station-wireless-charging-breakthrough, accessed: 2023-10-13

positioning was studied in [10] and [11], where the drone placement/trajectory and resource allocation were jointly optimized for a laser-powered drone acting as a flying base station (BS) serving a multitude of users with the aim of total flight time and communication data rate maximization [10], and, similarly in [11]. Furthermore, optimization of power management is investigated in [14], [20], while energy allocation and task offloading were optimized in a UAV-aided mobile edge cloud continuum in [14]. Furthermore, the operating time was optimized by exploiting the battery dynamics and opportunistically minimizing the propulsion energy consumption by resting on the roofs of buildings [20]. Moreover, many recent studies have considered both information and energy relay among airborne nodes providing wireless coverage [12], [16], [17], [18]. A weighted sum of laser power data transmission efficiencies was maximized in [12] via trajectory and power optimization. A different metric is studied in [16], where the focus is on minimizing the sum of the UAVs and the robots served decoding errors to enable ultra-reliable low-latency communications. In terms of energy relaying, in [17], [18], the authors studied bi-level airborne networks where UAVs at higher layers wirelessly charge their lower layer counterparts. In these works, the sum-energy received by all BS UAVs is maximized via trajectory optimization, while the overall network energy consumption is minimized by charging time portion and trajectory tuning in [17] and [18], respectively.

It is well known that IoT devices require almost absolute passiveness, which is a challenging feature to achieve. However, it has motivated many research efforts to study airborne aided backscatter communications (backCom), where each passive device (PD) modulates the incident wave generated by the carrier emitter (CE) with its message [21], [22], [23], [24], [25], [26], [27], [28], [29], [30], [31], [32]. In particular, network energy efficiency and throughput maximization have received considerable attention in numerous works [21], [22], [23], [24]. In these works, the degrees of freedom varied between UAV trajectory, static collection locations, CE power, reflection coefficients of the PDs, energy harvesting time fractions, and PDs scheduling. Moreover, different energy and data transmission schemes were studied where both backscattering and active transmissions are exploited and optimized, with different configurations for backscattering as monostatic, bistatic and ambient backscattering, realized by having CEs at both UAVs and ground stations. Furthermore, the maximization of the minimum rate among the PDs, and the overall throughput, for both direct transmission setups and opportunistic relaying based on the availability of direct links, was considered in [27], [29], [32].

In parallel, some research efforts have been directed towards improving the fidelity of the data collected in such semi-passive setups [26], [28], [30], [31]. These works aimed at minimizing the age of information, mean square error of the sensors reconstructed observations, maximizing the ratio between number of correctly decoded bits and the flight-time duration to collect the sensors data, and maximizing the uplink fair-secrecy-rate in the presence of a multitude of eavesdroppers. In addition, recently, reconfigurable intelligent surfaces (RIS) have been exploited to enhance backCom [33] by improving the channel gain either in a totally passive or quasi-active manner [34]. It has been shown that the recently introduced active RIS scheme outperforms its passive counterpart for small number of reflecting elements [35], [36], which promotes it as a good candidate for IoT networks.

At the intersection of research between UAV backscatter communications and laser-powered UAVs, the authors of [37] maximize the number of served IoT nodes by tuning (*i*) the access links transmitted power, (*ii*) time fractions for laser charging, and (*iii*) multiple access of different users. On one hand, fixed-wing UAVs enjoy relatively low required propulsion power, deployment flexibility, and their endurance can be boosted when employed in conjunction with laser power beaming. On the other hand, power beacon sources such as tethered helikites and aerostats retain a high probability of line-of-sight (LoS) with ground terminals and affordable deployment costs [38]. Therefore, the synergy of the aforementioned technologies positions them as a promising solution for IoT data collection systems in a multitude of scenarios, such as post-disaster communications in urban areas, monitoring and prediction of the progression of wildfires, and remote deployment coverage, to name a few. To the best of our knowledge, this is the first work to study the overall laser energy minimization for a laser-powered fixed-wing UAV collecting data via bistatic backscattering, which provides better communication ranges and lower terminal complexity compared with monostatic counterparts, from IoT PDs [39], [40]. In addition, it reduces the system dependence on batteries to a single battery empowering the radiation source on board the power beacon source (e.g., helikite) which, in turn, enables PDs to communicate with the UAV through bistatic backscattering. This comes at the cost of the need for accurate laser beam pointing and tracking systems.

A. MAIN CONTRIBUTIONS

The main contributions of this work include:

- exploiting the merits of both static and moving aerial platforms to provide a flexible remotely powered and operated data collection system that serves a field of passive IoT devices,
- presenting the minimum required laser output optical power needed to empower UAVs over different ranges and weather conditions while accounting for poiniting error losses,
- deriving novel SCA-compatible upper bounds for the product of two positive convex/concave functions, that were heavily exploited to solve both the unspecified time horizon i) aggregate data maximization, and ii) overall laser energy consumption minimization problems,

- the derived bounds enabled us to solve the previously mentioned problems using single-block SCA, despite the intricacies associated with the probabilistic LoS channel model and path discretization formulation, which guarantees covergence to a Karush-Kuhn-Tucker (KKT) solution, unlike the widely-adopted block coordinate descent approach,
- providing a novel asymptotically tight approximation for the UAV acceleration magnitude under path discretization and account for the acceleration magnitude effect on propulsion energy consumption, in addition to proposing a low-complexity solution for the aggregate data maximization problem,
- conducting a comprehensive set of simulations to show the optimization gains behavior against different critical system parameters such as the power beacon height, minimum data requirement, PDs locations, and laser source locations.

B. PAPER NOTATIONS AND ORGANIZATION

Notations: In this paper, we represent vectors by small bold letters as $\boldsymbol{a}$, where $\boldsymbol{a} = [a_x \ a_y \ a_z]^{\mathrm{T}}$, with a_x, a_y, and a_z representing its x, y, and z coordinates, respectively, and $(.)^{\mathrm{T}}$ represents the transpose operator. Furthermore, we use $||.||_2$ to denote the ℓ_2-norm, while we use $|.|$ to represent the absolute value of a scalar, or the Lebesgue measure of a set. $\mathbb{I}(C)$ represents an indicator function where $\mathbb{I}(C) = 1$ if the condition C is satisfied and $\mathbb{I}(C) = 0$, otherwise. We use calligraphic fonts to represent symbols for sets. The rest of this paper is organized as follows: first, we detail the adopted system and channel models in Section II. We then provide a mathematical formulation for joint trajectory optimization and resource allocation in Section III. Next, we propose a detailed SCA-based solution of the data maximization problem in Section IV and discuss the problem feasibility requirements in Section V. Then, we present the SCA-based solution of the laser energy minimization SCA solution, and then we propose a low-complexity solution for the collected data maximization problem in Section VI, followed by a set of extensive simulations to highlight the system dynamics and assess its performance in Section VII. Finally, the paper is concluded in Section VIII.

II. SYSTEM MODEL

In this work, we consider a laser-powered fixed-wing UAV traveling from a departure point 'A' towards a destination point 'B' at a fixed altitude H. Contrary to most of the existing literature, the flying time is not predetermined and therefore we adopt the path discretization approach [41]. Accordingly, we assume that the UAV path consists of N_{W} way points, excluding 'A' and 'B', with a maximum distance between consecutive way points of Δ_M. Specifically, Δ_M is set to guarantee negligible parameter variations between successive trajectory points. Hence, N_{W} is selected as $\lceil L_{\mathrm{UB}}/\Delta_M \rceil - 1$ to maintain the accuracy of the path discretization approximation, where L_{UB} represents the maximum allowed total flight distance. To this end, the UAV's location at the n-th way point is given by $\boldsymbol{q}^{\mathrm{u}}[n] = [q^{\mathrm{u}}_{\mathrm{x}}[n] \quad q^{\mathrm{u}}_{\mathrm{y}}[n] \quad H]^{\mathrm{T}}$ m with the origin assumed to be located right below 'A' on the ground plane. In addition, we denote by $\boldsymbol{v}[n] = [v_{\mathrm{x}}[n] \ \ v_{\mathrm{y}}[n] \ \ 0]^{\mathrm{T}}$ m/sec. and $\boldsymbol{a}[n] = [a_{\mathrm{x}}[n] \quad a_{\mathrm{y}}[n] \quad 0]^{\mathrm{T}}$ m/sec^2 the velocity and acceleration vectors at the $n-$th way point, respectively, where $v_- \leq ||\boldsymbol{v}||_2 \leq v_+$, and $||\boldsymbol{a}||_2 \leq a_{\mathrm{M}}$.

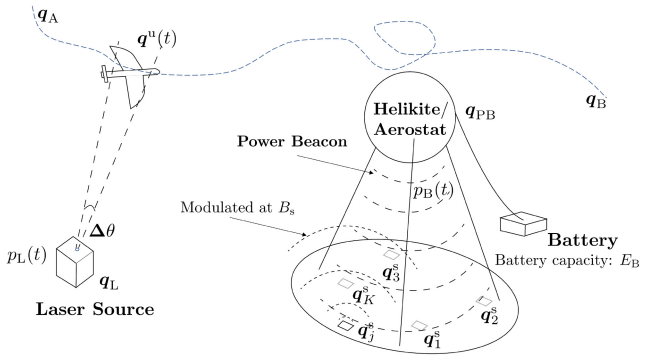

FIGURE 1. System Model.

The network features K terrestrial PDs whose data is continuously collected by the UAV via backscatter communications in a time division multiple access (TDMA) fashion. Specifically, the location of the i-th PD is given by $\boldsymbol{q}^{\mathrm{s}}_i = [q^{\mathrm{s}}_{\mathrm{x},i} \quad q^{\mathrm{s}}_{\mathrm{y},i} \quad 0]^{\mathrm{T}}$ m. In addition, a power beacon source is placed at 'PB' with coordinates $\boldsymbol{q}_{\mathrm{PB}} = [x_{\mathrm{PB}} \ \ y_{\mathrm{PB}} \ \ z_{\mathrm{PB}}]^{\mathrm{T}}$, generating an unmodulated carrier signal at a carrier frequency of f_{c} Hz with an instantaneous radiated power of $p_{\mathrm{B}}[n]$, that should not exceed a maximum limit $p^{\max}_{\mathrm{B}}$. Without loss of generality, we assumed that such a source could be a tethered aerostat or a helikite, although other possibilities include, for example, mobile deployable towers. Such a helikite/aerostat could be fixed with three tension wires that are controlled by motors to counteract wind effects and keep its position relatively stable as studied in [42]. The PDs scatter the impinging waves from the power beacon source while modulating them with their generated data, where the modulation bandwidth is denoted by B_{s} as depicted in Fig. 1. The power beacon transmitter is electrically powered via a battery having a capacity of E_{B} Joules.

The laser station, assumed to be located at point 'L' defined by $\boldsymbol{q}_{\mathrm{L}} = [x_{\mathrm{L}} \quad y_{\mathrm{L}} \quad z_{\mathrm{L}}]^{\mathrm{T}}$ m, radiates $p_{\mathrm{L}}[t]$ W of optical power with a maximum value of $p^{\max}_{\mathrm{L}}$ W. In addition, the UAV carries a photoelectric converter, of area A_{PD} m^2 and photodetector responsivity R_{PD} A/W. The photodetector aperture is assumed to be perfectly oriented orthogonal to the line joining the laser source and the photoelectric converter center throughout the whole flight duration to ensure maximum power transfer. Moreover, we assume that the laser source is attached to an APT system that supports wide angular range and fast switching response to handle the potential laser narrow beam interruptions and agile UAV

dynamics. Such features can be best supported by hybrid gimbal and fast switching mirror or a hybrid radio frequency (RF)-FSO APT system [5].

A. LASER BEAMING IMPERFECTIONS

It is evident that the laser beam's total radiated power experiences many forms of losses along its path of propagation to the photovoltaic converter onboard the UAV. First, a portion of the emitted optical power is scattered and absorbed by atmospheric particles, e.g., rain, fog or smoke to mention a few. Second, the temperature variations along the beam propagation path result in a variable refractive index and consequently beam scintillation, a.k.a turbulence, which reduces the power captured by the receiving aperture. In addition, due to the imperfect estimation of the UAV's location, mechanical friction, and vibration of the used pointing and tracking system, pointing losses need to be accounted for. Finally, the laser-emitted power is distributed over a larger area as the beam propagates away from the laser aperture. This beam spreading leads to a decrease in the power being absorbed by the photoelectric converter, denoted by geometric losses. This loss is totally determined by the aperture size, the beam divergence angle, and the separation distance between the laser and the photoelectric converter apertures.

The extinction coefficients associated with absorption and scattering losses can be quantified for rain, snow [43], fog, and smoke [44], respectively, as

$$\alpha_{\text{Rain}} = 0.1076 \times 10^{-3} \ln(10)\, R_r^{2/3}, \tag{1}$$

$$\alpha_{\text{Snow}} = 0.1 \times 10^{-3} \ln(10)\, a\, S^b, \tag{2}$$

$$a = 5.42 \times 10^{-5}\lambda + 5.4958776, \quad b = 1.38, \tag{3}$$

$$\alpha_{\text{Fog}} = \frac{0.17 \times 10^{-3} \ln(10)}{V} \left(\frac{\lambda}{\lambda_o}\right)^{-q_{\text{Fog}}(\lambda)}, \tag{4}$$

$$\alpha_{\text{Smoke}} = \frac{0.17 \times 10^{-3} \ln(10)}{V} \left(\frac{\lambda}{\lambda_o}\right)^{-q_{\text{Smoke}}(\lambda)}, \tag{5}$$

$$q_{\text{Fog}}(\lambda) = 0.1428\lambda - 0.0947, \tag{6}$$

$$q_{\text{Smoke}}(\lambda) = 0.8467\lambda - 0.5212. \tag{7}$$

where R_r is the rain rate in mm/h, S is the snow rate in mm/h, λ represents the laser wavelength in m, V is the laser beam visibility in km, and λ_o is the visibility reference wavelength in m. In addition, the turbulence losses can be expressed as

$$L_{\text{Tur}} = 10^{-a_{\text{scin}} ||\boldsymbol{q}^{\text{u}}[n] - \boldsymbol{q}_{\text{L}}||_2 / 10^4}, \tag{8}$$

where

$$a_{\text{scin}} = 2\sqrt{23.17 \left(\frac{2\pi}{\lambda}\right)^{7/6} C_n^2\, ||\boldsymbol{q}^{\text{u}}[n] - \boldsymbol{q}_{\text{L}}||_2^{11/6}}, \tag{9}$$

C_n^2 is 10^{-16} for weak turbulence, 10^{-14} for moderate turbulence, and 10^{-13} for strong turbulence. Finally, the pointing losses can be expressed as [45, eq. (2.21)]

$$L_{\text{P}} = e^{-8\left(\frac{\theta_{\text{err}}}{\theta_{\text{div}}}\right)^2}, \tag{10}$$

where θ_{err} represents the total angular misalignment error between the laser beam axis and the line joining the centers of the laser source and the photodetector apertures.

III. PROBLEM FORMULATION

With the aim of increasing the UAV's data collection capability, we now focus on maximizing the harvested data by the UAV from the PDs throughout its flight, having a maximum length L_{UB}. Hence, we are interested in finding the optimal values for (*i*) the UAV waypoint locations $\{\boldsymbol{q}^{\text{u}}[n]\}_{n=1}^{N_{\text{W}}}$, (*ii*) the time intervals between two successive trajectory points $\{\Delta t[n]\}_{n=1}^{N_{\text{W}}+1}$, and (*iii*) the radiated power profiles of the power beacon and the laser sources $\{p_{\text{B}}[n]\}_{n=1}^{N_{\text{W}}+1}$ and $\{p_{\text{L}}[n]\}_{n=1}^{N_{\text{W}}+1}$, respectively.

We adopt the probabilistic LoS channel model to account for potential blockage effects in different environments [46], while small scale fading effects are ignored. Consequently, the average collected data, to be maximized, can be expressed as

$$\bar{D} = \sum_{i=1}^{K} D_i,$$

$$D_i = \sum_{n=1}^{N_{\text{W}}+1} \frac{B_{\text{s}}}{K} \Delta t[n] \sum_{(\rho_1,\rho_2)\in\mathcal{P}} P^{\text{U}}_{\rho_1,i} P^{\text{B}}_{\rho_2,i} \log_2\left(1 + \frac{p_{\text{B}}[n]\zeta_{i,\rho_2}}{\mu_{\rho_1} d_{i,\text{U}}^{\alpha_{\rho_1}}[n]}\right), \tag{11}$$

where $\mathcal{P} = \{\text{L}, \text{N}\} \times \{\text{L}, \text{N}\}$ and $P^{\text{U}}_{\text{L},i}[n]$, $P^{\text{B}}_{\text{L},i}$ represent the LoS probability for the link between the $i-$th PD and the UAV, and the $i-$th PD and the power beacon, respectively, while $P^{\text{U}}_{\text{N},i}[n] = 1 - P^{\text{U}}_{\text{L},i}[n]$, and $P^{\text{B}}_{\text{N},i} = 1 - P^{\text{L}}_{\text{L},i}$. In addition, $p_{\text{B}}[n]$ is the radiated power from the power beacon source when the UAV reaches the $n-$th way point, $\mu_{\text{L}} = 1$, μ_{N} depends on the environment characteristics, $d_{i,\text{U}}$ is the distance between the UAV and $i-$th PD, and variables α_{L} and α_{N} represent the channel path loss exponents for LoS and Non-LoS cases, respectively. Finally, $\zeta_{i,\text{L}}$ and $\zeta_{i,\text{N}}$ represent the $i-$th PD cascaded channel-gain-to-noise-ratio excluding the distance for the LoS and Non-LoS power beacon, respectively, and can be expressed as [39]

$$\zeta_{i,\rho} = \Gamma^{-1} \mu_\rho^{-1} \beta_o^2 G \eta_{\text{s}} d_{i,\text{B}}^{-\alpha_\rho} / \sigma^2, \quad \forall i \in \{1, \ldots, K\},$$

where Γ is the signal-to-noise ratio gap, β_o is the path loss factor for both UAV-PD and PD-PB links at a reference distance of 1 m, and G is the product of transmitter, receiver, and square of the PD antenna gains. Moreover, η_{s} denotes the scattered power portion, $d_{i,\text{B}}$ is the distance between the power beacon source and the $i-$th PD, and σ^2 is the noise power at the receiver. The LoS probabilities of the UAV-$i-$th PD, and the $i-$th PD - PB links are, respectively, given as

$$P^{\text{U}}_{\text{L},i}[n] = P_{\text{L}}\left(\theta_i^{\text{U}}[n]\right), \quad \forall i \in \{1, \ldots, K\}, \tag{12}$$

$$P^{\text{B}}_{\text{L},i} = P_{\text{L}}\left(\theta_i^{\text{B}}\right) \quad \forall i \in \{1, \ldots, K\}, \tag{13}$$

$$P_{\text{L}}(x) = C_1 + \frac{C_2}{1 + e^{-(B_1 + B_2 x)}}, \tag{14}$$

where C_1, C_2, B_1, and B_2 are environment dependent constants [46], [47]. $\theta_i^{\mathrm{U}}[n]$ is the elevation angle between the UAV at the $n-$th way point and the $i-$th PD while θ_i^{B} is the elevation angle between the $i-$th PD and the power beacon source with $P_{\mathrm{N},i}^{\chi} = 1 - P_{\mathrm{L},i}^{\chi}$.

In addition, we adopt the non-linear model given by [48, eq. (2.21)] to represent the harvested power by the UAV:

$$P_{\mathrm{H}}[n] = 0.75\mathrm{V_t} x[n] \ln(1 + x[n]/\mathrm{I_o}), \tag{15}$$

where $\mathrm{V_t}$ represents the thermal voltage, $x[n]$ is the photocurrent generated at the photodiode by the impinging laser beam, and $\mathrm{I_o}$ is the dark saturation current with $x[n]$ given by [49]

$$x[n] = A_{\mathrm{PD}} R_{\mathrm{PD}} p_{\mathrm{L}}[n] e^{-\alpha d_{\mathrm{L}}^{\mathrm{u}}[n]} r_{\mathrm{L}}^{-2}[n] L_{\mathrm{Tur}} L_{\mathrm{P}}, \tag{16}$$

where α is the extinction coefficient, $\mathrm{D_o}$ is the laser beam diameter at the aperture, $\Delta\theta$ is the laser angular beam deviation, $d_{\mathrm{L}}^{\mathrm{u}}[n] = \|\boldsymbol{q}^{\mathrm{u}}[n] - \boldsymbol{q}_{\mathrm{L}}\|_2$, and $r_{\mathrm{L}}[n] = \|\mathrm{D_o} + \Delta\theta d_{\mathrm{L}}^{\mathrm{u}}[n]\|_2$. In terms of the UAV's propulsion power at the $n-$th way point, the following approximation is adopted, by replacing $||\boldsymbol{a}||_2$ in [50, eq. (12)] with a_{M}

$$\tilde{p}_{\mathrm{R}}[n] = c_1 ||\boldsymbol{v}[n]||_2^3 + \frac{c_2}{||\boldsymbol{v}[n]||_2} \left(1 + \frac{a_{\mathrm{M}}^2}{g^2}\right), \tag{17}$$

where c_1 and c_2 are constants that depend on the UAV's characteristics and the experienced wind properties. Consequently, the harvested data maximization problem can be expressed as

$$\begin{aligned}
(\mathbf{P1}) \quad & \max_{\boldsymbol{Q}, \boldsymbol{\Delta t}, \boldsymbol{p}_{\mathrm{B}}, \boldsymbol{p}_{\mathrm{L}}} \quad \bar{D} \\
\text{S.t.} \quad & \\
\mathrm{C1}: \; & \left|\left|\boldsymbol{q}^{\mathrm{u}}[n] - \boldsymbol{q}^{\mathrm{u}}[n-1]\right|\right|_2 \leq \Delta_{\mathrm{M}}, \qquad \forall n \in \mathcal{N}_1, \\
\mathrm{C2}: \; & v_- \leq \|\boldsymbol{v}[n]\|_2 \leq v_+, \; \forall n \in \mathcal{N}_1, \\
\mathrm{C3}: \; & \|\boldsymbol{a}[n]\|_2 \leq a_{\mathrm{M}}, \; \forall n \in \mathcal{N}_2, \\
\mathrm{C4}: \; & \tilde{p}_{\mathrm{R}}[n] \leq P_{\mathrm{H}}[n], \forall n \in \mathcal{N}_1, \\
\mathrm{C5}: \; & \sum_{n=1}^{N_{\mathrm{W}}+1} \Delta t[n] p_{\mathrm{B}}[n] \leq \bar{E}_{\mathrm{B}}, \\
\mathrm{C6}: \; & p_{\mathrm{B}}[n] \leq p_{\mathrm{B}}^{\max}, \; p_{\mathrm{L}}[n] \leq p_{\mathrm{L}}^{\max} \; \forall n \in \mathcal{N}_1, \\
\mathrm{C7}: \; & p_{\mathrm{B}}[n] \geq 0, p_{\mathrm{L}}[n] \geq 0, \Delta t[n] \geq 0, \; \forall n \in \mathcal{N}_1, \\
\mathrm{C8}: \; & D_i \geq D_{\min}^{\mathrm{ind}} \quad \forall i \in \{1, \ldots, K\},
\end{aligned}$$

where (i) $\boldsymbol{Q}$ represents the set of way-point locations $\{\boldsymbol{q}^{\mathrm{u}}[n]\}_{n=1}^{N_{\mathrm{W}}}$, (ii) $\boldsymbol{\Delta t}$ represents the set of interval durations between the UAV successive transitions $\{\Delta t[n]\}_{n=1}^{N_{\mathrm{W}}+1}$, (iii) $\boldsymbol{p}_{\mathrm{B}}$ is the set of radiated power variables by the power beacon source at the trajectory points $\{p_{\mathrm{B}}[n]\}_{n=1}^{N_{\mathrm{W}}+1}$, and (iv) $\boldsymbol{p}_{\mathrm{L}}$ represents the radiated laser power variables $\{p_{\mathrm{L}}[n]\}_{n=1}^{N_{\mathrm{W}}+1}$. Moreover, $\mathcal{N}_1 = \{1, \ldots, N_{\mathrm{W}}+1\}, \mathcal{N}_2 = \{2, \ldots, N_{\mathrm{W}}+1\}$, and we enforce initial and final UAV positions through $\boldsymbol{q}[0] = \boldsymbol{q}_{\mathrm{A}}$ and $\boldsymbol{q}[N_{\mathrm{W}}+1] = \boldsymbol{q}_{\mathrm{B}}$, respectively. Finally, $\bar{E}_{\mathrm{B}} = E_{\mathrm{B}}/\eta_{\mathrm{rad}}$, with η_{rad} being the ratio between the radiated power from the beacon transmitter to the supplied power.

In the previous formulation, C1 ensures a minimum path discretization accuracy while C2 imposes the minimum and maximum speed constraints of the UAV. In addition, C3 enforces the maximum acceleration magnitude whereas C4 ensures that the propulsion power needed by the UAV is supplied by the harvested power. Moreover, C5 embodies the limited battery capacity of the power beacon source, where the total radiated energy throughout the UAV's flight cannot exceed a certain threshold. Furthermore, the box constraints in C6 and C7 enforce a maximum power restriction for both radiation sources and positiveness of the radiated powers and the UAV's inter-way-points durations, respectively. Finally, C8 guarantees that each PD transfers at least $D_{\min}^{\mathrm{ind}}$ bits throughout the UAV's flight.

Following an approach similar to that of [46], we lower bound $\bar{D}$ by neglecting the NLoS contribution terms in (11), due to the huge channel magnitude gap with respect to the pure LoS term, to get $\bar{D}_{\mathrm{LB}}$ given by

$$\begin{aligned}
\bar{D}_{\mathrm{LB}} &= B_{\mathrm{s}}/(K \ln(2)) \sum_{i=1}^{K} \sum_{n=1}^{N_{\mathrm{W}}+1} \bar{D}_{\mathrm{LB},i}[n], \\
\bar{D}_{\mathrm{LB},i}[n] &= \Delta t[n] P_{\mathrm{L},i}^{\mathrm{U}}[n] P_{\mathrm{L},i}^{\mathrm{B}} \ln\left(1 + p_{\mathrm{B}}[n] \zeta_{i,\mathrm{L}} d_{i,\mathrm{U}}^{-\alpha_{\mathrm{L}}}[n]\right).
\end{aligned} \tag{18}$$

To tackle the non-convexity of (**P1**), we first adopt the following change of variables $\tilde{p}_{\mathrm{B}}[n] = \Delta t[n] p_{\mathrm{B}}[n] \;\; \forall n$. Moreover, $\|\boldsymbol{a}[n]\|_2$ in C3 is substituted by $\|\tilde{\boldsymbol{a}}[n]\|_2 = \|\boldsymbol{q}^{\mathrm{u}}[n] - 2\boldsymbol{q}^{\mathrm{u}}[n-1] + \boldsymbol{q}^{\mathrm{u}}[n-2]\|_2/\Delta t^2[n]$. Note that the previous expression is reached by replacing $\Delta t[n-1]$ with $\Delta t[n]$, which is an asymptotically tight approximation as N_{W} grows indefinitely, check Appendix A for proof. Also, it is worth mentioning that the optimal allocation for the laser power is $p_{\mathrm{L}}^*[n] = p_{\mathrm{L}}^{\max} \;\; \forall n$, as increasing $p_{\mathrm{L}}[n] \;\; \forall n$, widens the feasibility space. Hence, we solve the optimization problem ($\tilde{\mathbf{P}}\mathbf{1}$), which is an approximation of (**P1**):

$$\begin{aligned}
\left(\tilde{\mathbf{P}}\mathbf{1}\right) \quad & \max_{\boldsymbol{Q}, \boldsymbol{\Delta t}, \tilde{\boldsymbol{p}}_{\mathrm{B}}} \quad \bar{D}_{\mathrm{LB}} \\
\text{S.t.} \quad & \\
\mathrm{C1, C2, C3'}: \; & \|\tilde{\boldsymbol{a}}[n]\|_2 \leq a_{\mathrm{M}}, \quad \forall n \in \mathcal{N}_2, \\
\mathrm{C4'}: \; & \tilde{p}_{\mathrm{R}}[n] \leq \hat{P}_{\mathrm{H}}[n], \; \forall n \in \mathcal{N}_1, \\
\mathrm{C5'}: \; & \sum_{n=1}^{N_{\mathrm{W}}+1} \tilde{p}_{\mathrm{B}}[n] \leq \bar{E}_{\mathrm{B}}, \mathrm{C6'}: \tilde{p}_{\mathrm{B}}[n] \leq \Delta t[n] p_{\mathrm{B}}^{\max}, \forall n \in \mathcal{N}_1, \\
\mathrm{C7'}: \; & \tilde{p}_{\mathrm{B}}[n] \geq 0, \Delta t[n] \geq 0, \; \forall n \in \mathcal{N}_1, \\
\mathrm{C8}: \; & D_i \geq D_{\min}^{\mathrm{ind}} \quad \forall i \in \{1, \ldots, K\},
\end{aligned}$$

where $\hat{P}_{\mathrm{H}}[n] = P_{\mathrm{H}}[n]|_{p_{\mathrm{L}}[n]=p_{\mathrm{L}}^{\max}}$.

A. UAV LASER CHARGING FEASIBILITY

Before delving into the solution details, the feasibility of laser power beaming for fixed-wing UAVs under different weather conditions is worth discussion. To keep the UAV aloft, the laser beam has to deliver the least propulsion power needed for the desired coverage range, which can be well approximated by [51]

$$p_{\min}^{\mathrm{Pr}} = a_1 v_{\mathrm{em}}^3 + \frac{a_2}{v_{\mathrm{em}}} \left(1 + a_{\mathrm{M}}^2/g^2\right), \tag{19}$$

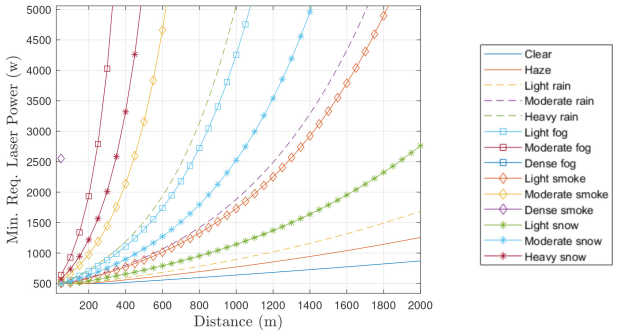

FIGURE 2. Minimum laser power to keep the UAV aloft indefinitely. (The parameter values for this figure are the default ones in table 1).

$$v_{\text{em}} = \left(\frac{a_2\left(1 + a_{\text{M}}^2/g^2\right)}{3a_1} \right)^{\frac{1}{4}}. \tag{20}$$

Towards this end, we study the minimum required laser output optical power to keep the UAV flying for different mission range requirements as shown in Fig. 2. Specifically, the results presented in such figure show that 1 KW of output laser power is sufficient to cover more than 2 Km under clear weather conditions. However, in the presence of haze the range decreases to 1.5 Km, 1.2 Km with light rain, and 800 m under light snow conditions. Although those ranges are much larger than what tethered drones can offer, under severe weather conditions, e.g., heavy fog and smoke, laser power beaming may not be a viable solution.

IV. AGGREGATE DATA MAXIMIZATION VIA SCA

To reach a KKT solution for ($\tilde{\mathbf{P1}}$), certain manipulations are needed for the non-convex terms. Particularly, we first derive locally tight, gradient matching, concave lower and convex upper bounds for the non-convex terms of ($\tilde{\mathbf{P1}}$), which are provided in Appendix B, to construct the convex problem (P2) expressed as

$$\begin{aligned}
(\mathbf{P2}) \quad & \max_{\boldsymbol{Q}, \boldsymbol{\Delta t}, \tilde{\boldsymbol{p}}_{\text{B}}} \quad \sum_{i=1}^{K} \sum_{n=1}^{N_{\text{W}}+1} \tilde{D}_{\text{LB},i}[n] \\
\text{s.t.} \quad & \\
& \text{C1, C2b, C5}', \text{C6}', \text{C7}', \\
& \text{C4}'' : \hat{p}_{\text{R}}[n] \leq \tilde{P}_{\text{H}}[n], \ \forall n \in \mathcal{N}_1, \\
& \text{C2a}' : \tilde{s}[n] \geq v_- \Delta t[n], \quad \forall n \in \mathcal{N}_1, \\
& \text{C2b} : \|\boldsymbol{q}[n] - \boldsymbol{q}[n-1]\|_2 \leq v_+ \Delta t[n], \ \forall n \in \mathcal{N}_1, \\
& \text{C3}'' : \|\boldsymbol{q}[n] - 2\boldsymbol{q}[n-1] + \boldsymbol{q}[n-2]\|_2 \leq a_{\text{M}} \Delta \tilde{t}[n], \forall n \in \mathcal{N}_2, \\
& \text{C8}' : \sum_{n=1}^{N_{\text{W}}+1} \tilde{D}_{\text{LB},i}[n] \geq D_{\min}^{\text{ind}}, \ \forall i \in \{1, \ldots, K\}.
\end{aligned}$$

Then, we employ the SCA algorithm to solve ($\tilde{\mathbf{P1}}$) by solving a different (P2) instance at each SCA iteration, until convergence is reached as shown in Algorithm 1. It is worth mentioning that Algorithm 1 incurs an iteration complexity of $\mathcal{O}(I_{\text{SCA}}(4N_{\text{W}} + 2)^{3.5})$, where I_{SCA} represents the number of outer iterations needed by the SCA approach to converge.

Algorithm 1 Aggregate Data Maximization via SCA

1: **Initialize** $\boldsymbol{Q}^o$, $\boldsymbol{\Delta t}^o$, $\boldsymbol{p}_{\text{B}}^o$, Relative Error
2: **while** Relative Error $\geq \epsilon_{\text{ener.}}$ **do**
3: **Solve** (**P2**) for $\boldsymbol{Q}$, $\boldsymbol{\Delta t}$, $\boldsymbol{p}_{\text{B}}$ via interior point method.
4: Relative Error $\leftarrow \left|\bar{D}_{\text{LB}} - \bar{D}_{\text{LB}}^o\right| / D_{\text{LB}}^o$
5: $\boldsymbol{Q}^o \leftarrow \boldsymbol{Q}$, $\boldsymbol{\Delta t}^o \leftarrow \boldsymbol{\Delta t}$, $\boldsymbol{p}_{\text{B}}^o \leftarrow \boldsymbol{p}_{\text{B}}$
6: **end while**

V. LASER ENERGY MINIMIZATION

On the other performance end, energy expenditure is of utmost importance. Hence, the minimization of the laser energy expenditure over the flight that governs a minimum amount of collected data set by the mission goals is formulated as

$$\begin{aligned}
(\mathbf{P3}) \quad & \min_{\boldsymbol{Q}, \boldsymbol{\Delta t}, \boldsymbol{p}_{\text{B}}, \boldsymbol{p}_{\text{L}}} \quad \sum_{i=1}^{K} \sum_{n=1}^{N_{\text{W}}+1} p_{\text{L}}[n] \Delta t[n] \\
\text{s.t.} \quad & \\
& \text{C1–C8}, \\
& \text{C9} : \bar{D} \geq D_{\min}.
\end{aligned}$$

The non-convexity of the previous problem is evident as it shares all the constraints of (**P1**) along with the non-convex objective function formed by the sum of bilinear terms. To guarantee a KKT point solution, we iteratively solve (**P3**) using the single-block SCA approach, and, in particular by solving the convex problem ($\tilde{\mathbf{P3}}$) at each iteration.

$$\begin{aligned}
\left(\tilde{\mathbf{P3}}\right) \quad & \min_{\boldsymbol{Q}, \boldsymbol{\Delta t}, \tilde{\boldsymbol{p}}_{\text{B}}, \tilde{\boldsymbol{p}}_{\text{L}}} \quad \sum_{i=1}^{K} \sum_{n=1}^{N_{\text{W}}+1} \frac{1}{4} \Big((p_{\text{L}}[n] + \Delta t[n])^2 + \left(p_{\text{L},o}[n] - \Delta t_o[n]\right)^2 \\
& \qquad\qquad -2\left(p_{\text{L},o}[n] - \Delta t_o[n]\right)\left(p_{\text{L}}[n] - \Delta t[n]\right) \Big) \\
\text{s.t.} \quad & \\
& \text{C1, C2a}', \text{C2b, C5}', \text{C6}', \text{C7}', \text{C8}', \\
& \text{C4}'' : \hat{p}_{\text{R}}[n] \leq \tilde{P}_{\text{H},2}[n], \ \forall n \in \mathcal{N}_1, \\
& \text{C9}' : \sum_{i=1}^{K} \sum_{n=1}^{N_{\text{W}}+1} \tilde{D}_{\text{LB},i}[n] \geq D_{\min},
\end{aligned}$$

where $p_{\text{L},o}[n]$ represents the value of $p_{\text{L}}[n]$ in the previous SCA iteration, and $\tilde{P}_{\text{H},2}[n]$ represents an SCA-compatible lower bound for the instantaneous harvested energy when the instantaneous laser power is considered as a variable parameter, unlike $\tilde{P}_{\text{H}}[n]$.

$$\tilde{P}_{\text{H},2}[n] = a_o[n] + b_o[n]c_o[n]p_{\text{L}}[n] - b_o[n]d_o[n]f_n^{\text{UB}}[n], \tag{21}$$

where $a_o[n]$, $b_o[n]$, $c_o[n]$, and $d_o[n]$ are constants, and $f_n^{\text{UB}}[n]$ is a convex function of all the optimization parameters.[2]

It is worth mentioning that the feasibility of (**P3**) can be determined by solving ($\tilde{\mathbf{P1}}$) optimally, and checking if the optimal amount of the collected data surpasses $D_{\min}$.

Finally, the solution of (**P3**) proceeds as depicted in Algorithm 2, where E_{L} represents the laser energy expenditure throughout the whole flight evaluated using the updated values of $\boldsymbol{Q}$, $\boldsymbol{\Delta t}$, $\boldsymbol{p}_{\text{B}}$, $\boldsymbol{p}_{\text{L}}$ whilst E_{L}^o is its previous iteration counterpart. In addition, Algorithm 2 incurs an

[2]The definitions of the constants and $f_n^{\text{UB}}[n]$ are all provided in Appendix B.

Algorithm 2 Laser Energy Minimization

Initialize $\boldsymbol{Q}^o$, $\boldsymbol{\Delta t}^o$, $\boldsymbol{p}_{\mathbf{B}}^o$, $\boldsymbol{p}_{\mathbf{L}}^o$, Relative Error
while Relative Error $\geq \epsilon_{\text{ener.}}$ **do**
  Solve (**P3**) for $\boldsymbol{Q}$, $\boldsymbol{\Delta t}$, $\boldsymbol{p}_{\mathbf{B}}$, $\boldsymbol{p}_{\mathbf{L}}$ via interior point method.
  Relative Error $\leftarrow \left|E_{\text{L}} - E_{\text{L}}^o\right| / E_{\text{L}}^o$
  $\boldsymbol{Q}^o \leftarrow \boldsymbol{Q}$, $\boldsymbol{\Delta t}^o \leftarrow \boldsymbol{\Delta t}$, $\boldsymbol{p}_{\mathbf{B}}^o \leftarrow \boldsymbol{p}_{\mathbf{B}}$, $\boldsymbol{p}_{\mathbf{L}}^o \leftarrow \boldsymbol{p}_{\mathbf{L}}$
end while

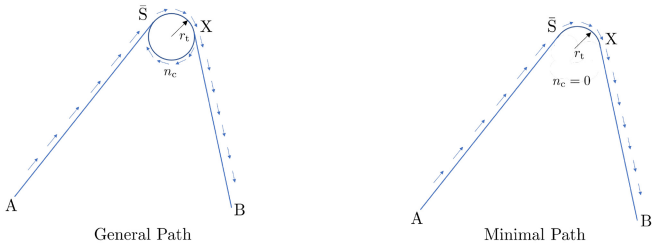

FIGURE 3. Simplified Trajectory Structure.

iteration complexity of $\mathcal{O}(I_{\text{SCA},2}(5N_{\text{W}}+3)^{3.5})$, where $I_{\text{SCA},2}$ represents the number of outer SCA iterations the algorithm takes to converge.

VI. LOW COMPLEXITY AGGREGATE DATA MAXIMIZATION

In this section, we provide a simpler way to find a feasible trajectory and power beacon radiated power profile aiming at maximizing the aggregate collected data by the UAV throughout its flight. It is clear that the aggregate data increases by lengthening the overall flight duration and by improving the channel gains between the UAV and the PDs. The former can be realized by slowing down the UAV as much as possible and elongating the path to the limit. On the other hand, the latter can be attained by keeping the UAV in close vicinity of the PDs.

In our simplified approach, we assume the UAV path is restricted to straight lines and circular arcs while moving at a constant speed v_{c}. To maintain the velocity vector continuity as a function of time, we enforce that the UAV transition from a linear path to a circular path is performed at a point where both path portions are tangential. Based on the previously mentioned preferences for the UAV trajectory with respect to aggregate data maximization, we propose the UAV path depicted in Fig. 3. In such a trajectory, the UAV moves in a straight line till it reaches the point right above the centroid of the sensors 'S̄' in the UAV flight plane. Then, it initiates a circular turn and concludes the turn at 'X' in a tangential straight line heading towards 'B' after completing the maximum possible number of cycles n_{c} over the PDs' region. To fully specify the trajectory, we need to determine the radius of turn r_{t} and the UAV's speed throughout the trajectory.

From an objective maximization perspective, it is favorable to reduce the UAV's speed and reduce the turn radius to keep close to the sensors and be able to complete larger number of cycles. Nonetheless, both actions might result in violating the power budget and acceleration magnitude requirements of the problem. Consequently, we first introduce a more restrictive version of the power budget constraint that simplifies the turn radius and speed search as

$$c_1 v_{\text{c}}^3 + \frac{c_2}{v_{\text{c}}}\left(1 + \frac{a_{\max}^2}{g^2}\right) \leq P_{\text{H}}(v), \tag{22}$$

$$v = p_{\text{L}}^{\max} L_{\text{D}}\left(\sqrt{\left(\max\left(d_{\bar{\text{S}}\bar{\text{L}}} + 2r_{\text{t}}, d_{\text{A}\bar{\text{L}}}, d_{\text{B}\bar{\text{L}}}\right)\right)^2 + (H - z_{\text{L}})^2}\right), \tag{23}$$

$$P_{\text{H}}(x) = 0.75 \text{V}_{\text{t}} x \ln(1 + x/\text{I}_{\text{o}}),$$
$$L_{\text{D}}(x) = A_{\text{PD}} R_{\text{PD}} \frac{e^{-\alpha x}}{(D_o + \Delta\theta x)^2},$$

where $d_{\bar{\text{S}}\bar{\text{L}}}$ is the distance between $\bar{\text{S}}$, and $\bar{\text{L}}$, which represent the projections of the sensors' centroid and the laser station locations in the UAV's flight plane, respectively. $d_{\text{A}\bar{\text{L}}}$ and $d_{\text{B}\bar{\text{L}}}$, are the lengths of the two segments 'A$\bar{\text{L}}$' and 'B$\bar{\text{L}}$', respectively. It is worth mentioning that the R.H.S of (23) is a lower bound on the power harvested at any given point in the trajectory. This lower bound is attained by upper bounding the distance between any point on the trajectory and the laser station.

The acceleration magnitude constraint is automatically satisfied for the straight segments of the trajectory for which the acceleration magnitude is nullified. Nonetheless, for the circular portion, the acceleration constraint reduces to [52]

$$\frac{v_{\text{c}}^2}{r_{\text{t}}} \leq a_{\max}. \tag{24}$$

It can be observed that, for $v_{\text{c}} \leq v_{\text{em}}$, (23) implies a lower bound on v_{c}. Similarly, (24) imposes a lower bound on the turn radius. Consequently, we reduce both v_{c} and r_{t}, by iteratively fixing one of them and finding the least feasible value for the other using (23) and (24), as detailed in Algorithm 3.

Now, the minimal UAV trajectory is fully specified by r_{t} and v_{c}. We propose that the UAV takes the maximum number of turns before it heads towards 'B'. Accordingly, n_{c} is expressed as

$$n_{\text{c}} = \left\lfloor \frac{L_{\text{UB}} - |\text{A}\bar{\text{S}}| - |\text{XB}|}{2\pi r_{\text{t}}} \right\rfloor. \tag{25}$$

Algorithm 3 Turn Radius and Trajectory Speed Tuning

Input $\boldsymbol{q}_{\text{A}}, \boldsymbol{q}_{\text{B}}, \boldsymbol{q}_{\bar{\text{S}}}, \boldsymbol{q}_{\text{L}}, H, p_{\text{L}}^{\max}, D_o, \Delta\theta, A_{\text{PD}}, R_{\text{PD}}, v_{\min}, a_{\max}$.
$v_{\text{c}} \leftarrow v_{\text{em}}$
Relative Error $\leftarrow \infty$
while Relative Error $\geq \epsilon_{\text{v}}$ **do**
  $r_{\text{t}} \leftarrow \frac{v_{\text{c}}^2}{a_{\max}}$
  $v^* \leftarrow \min_{v_{\min} \leq v \leq v_{\text{t}}} v$ s.t. $c_1 v^3 + \frac{c_2}{v}\left(1 + \frac{a_{\max}^2}{g^2}\right) \leq P_{\text{H}}\left(p_{\text{L}}^{\max} L_{\text{D}}\left(\sqrt{\bar{d}_{\text{UB}}^2 + \Delta H^2}\right)\right)$,
  where $\bar{d}_{\text{UB}} = \max\left(d_{\bar{\text{S}}\bar{\text{L}}} + 2r_{\text{t}}, d_{\text{A}\bar{\text{L}}}, d_{\text{B}\bar{\text{L}}}\right)$, $\Delta H = (H - z_{\text{L}})$.
  Relative Error $\leftarrow \frac{|v^* - v_{\text{c}}|}{v_{\text{c}}}$
end while

TABLE 1. Default simulation parameters.

$D_o = 10$ cm	$v_- = 3$ m/sec	$R_{\rm PD} = 1$ A/W	$\eta_{\rm s} = 0.043$
$\Delta\theta = 2 \times 10^{-5}$	$v_+ = 100$ m/sec	$A_{\rm PD} = 40$ cm^2	$K = 54$
$p_{\rm L}^{\max} = 700$ W	$a_{\rm M} = 5$ m/sec^2	$V_{\rm T} = 0.025$ V	$\Gamma = 6.6$
$\alpha = 10^{-6}$ m^{-1}	$p_{\rm B}^{\max} = 40$ W	$I_o = 10^{-14}$ A	$G = 10.25$
$\beta_o = 7 \times 10^{-4}$	$\bar{E}_{\rm B} = 2.9$ kJ	$B_2 = 0.0470$	$\alpha_{\rm N} = 3.5$
$\sigma^2 = -174$ dB	$B_{\rm s} = 10$ KHz	$L_{\rm UB} = 2.25$ km	$\alpha_{\rm L} = 2.5$
$C_1 = -0.63$	$C_2 = 1.63$	$B_1 = -0.4568$	$\mu_{\rm N} = 100$

At this point, the trajectory path is discretized by dividing it into equal length segments, where the number of segments is determined by $L_{\rm UB}$ and $N_{\rm W}$, as indicated in the previous sections. By plugging the derived trajectory into ($\tilde{\mathbf{P}}\mathbf{1}$), the power beacon radiated power profile is determined by

$$\text{(P4)} \ \underset{\mathbf{S.t.}}{\max_{\tilde{p}_{\rm B}}} \ \frac{B_{\rm s}}{K} \sum_{i=1}^{K} \sum_{n=1}^{N_{\rm W}+1} \Delta t[n] P_{{\rm L},i}^{\rm U}[n] P_{{\rm L},i}^{\rm B} \ln\left(1 + \frac{\zeta_{i,{\rm L}} \tilde{p}_{\rm B}[n]}{\Delta t[n] d_{i,{\rm U}}^{\alpha_{\rm L}}[n]}\right)$$
$$\text{C6}', \ 0 \le \tilde{p}_{{\rm B},n} \le p_{\rm B}^{\max}, \quad \forall n \in \{1, \ldots, N_{\rm W}+1\}$$

which is a convex problem that can be solved by solving its KKT system at a quadratic iteration complexity.[3]

VII. SIMULATION RESULTS

In this section, we assume default initial and final UAV locations defined by $\boldsymbol{q}_{\rm A} = [0 \ 0 \ 80]^{\rm T}$ m and $\boldsymbol{q}_{\rm B} = [1000 \ 1000 \ 80]^{\rm T}$ m, respectively, while the default laser source and the power beacon locations are $\boldsymbol{q}_{\rm L} = [1000 \ 0 \ 20]^{\rm T}$ m and $\boldsymbol{q}_{\rm PB} = [200 \ 600 \ 60]^{\rm T}$, respectively, although other locations would work as well. In addition, we assume that the PDs are placed evenly on 6 concentric circles on the ground around the power beacon, where the largest circle has a radius of 500 m. Moreover, the system parameters, summarized in Table 1, are set based on [10], [11], [39] with $f_{\rm c} = 900$ MHz, , $D_{\min}^{\rm ind} = 0$ and $g = 9.8$ m/sec^2. With the aim of providing a fair comparison, we also include different benchmark algorithms. Particularly, the five different solutions are: (*i*) the data maximization solution using SCA (DMSCA), (*ii*) the energy minimization solution using SCA (EMSCA), (*iii*) the low-complexity linear-circular-linear (LCL) solution (as explained in Section VI), (*iv*) the energy minimization solution using SCA with a constant speed constraint (EMCS), (*v*) the data maximization solution using SCA with a constant speed constraint (DMCS), and (*vi*) the straight path solution where the UAV directly flies from 'A' to 'B' and power allocation is done similar to 'LCL' while the UAV moves at the power minimizing speed. In the following simulations, the LCL solution is used to initialize the DMSCA, EMSCA, DMCS, and the EMCS solutions. Finally, the pointing errors due to the angular localization uncertainty and the pointing devices aiming errors are both assumed to be submicroradian contributing to a total angular pointing uncertainty $\theta_{\rm err} = 2$ μrad.

[3]The KKT solution is omitted for brevity.

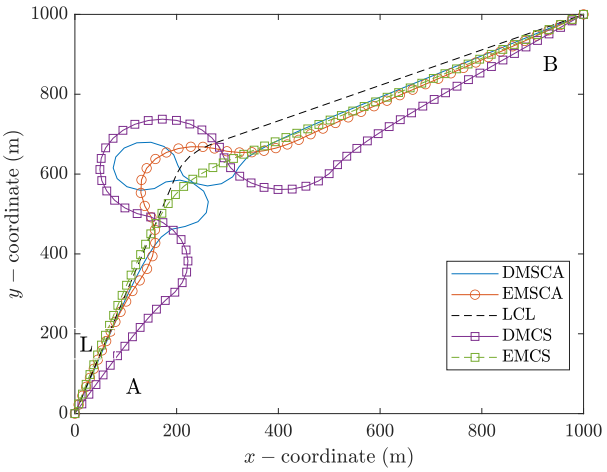

FIGURE 4. UAV Path.

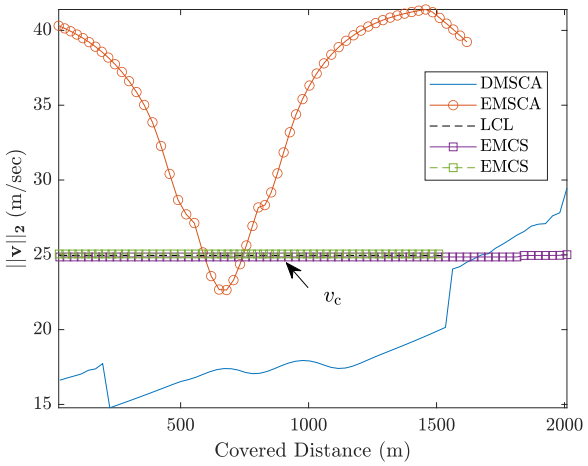

FIGURE 5. UAV Speed Profile.

A. SYSTEM DYNAMICS

To gain insights into the dynamic behavior of the considered aerial data collection system, we fix all system parameters and observe the UAV's path and instantaneous speed progression in Figs. 4 and 5, respectively. In addition, Figs. 6, and 7 present the power beacon source radiated power profile and laser radiated power throughout the flight, respectively. In these simulations, $D_{\min}$ is set to 0.9 Mbits which is sufficient for environmental/critical infrastructure monitoring IoT devices given the flight duration considered and the number of IoT PDs. In addition, we assume the laser is located at the UAV flight starting point at a large enough height to avoid LoS interruptions with the UAV, specifically $\boldsymbol{q}_{\rm L} = [0 \ 0 \ 20]^{\rm T}$ m. In what follows, we explain the trends in system dynamics associated with different solutions in these figures.

Fig. 4 shows that both DMSCA and DMCS solutions tend to lengthen the path portion closer to the PDs' deployment area, where the UAV experiences relatively high channel gains. On the other hand, EMSCA and EMCS solutions stratify the path as much as possible, as long as it could

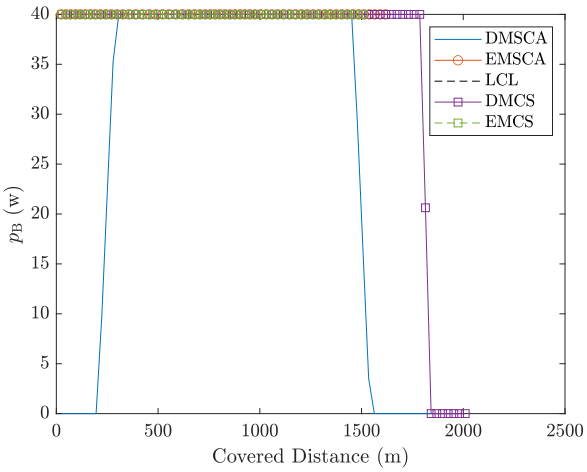

FIGURE 6. Power beacon radiated power profile.

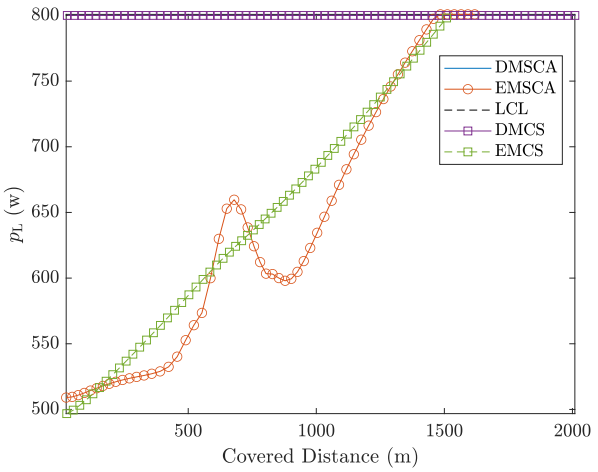

FIGURE 7. Laser radiated power profile.

satisfy the minimum collected data requirement. Basically, laser energy minimization pushes the UAV to reduce the laser radiated power and shorten the path as much as possible; hence, the path points are pulled towards the laser location, i.e., the less demanding the data collection requirement becomes, the more inclined the energy minimization path will be towards the laser location.

Speed profiles are plotted against the cumulative flight distance in Fig. 5. EMSCA and EMCS solutions exhibit unimodal behavior with a local minimum located at the PDs' deployment region. Basically, the solution tends to minimize the flight time by letting the UAV go as fast as the laser-radiated power could afford and reducing the UAV's speed to acquire enough time to satisfy the data collection requirement. Contrarily, DMSCA and DMCS tend to reduce the UAV's speed to the least velocity governed by the received laser power. It can be observed that a constant velocity, i.e., v_c, is higher than the speed profile of the DMSCA solution within the data transmission window owing to the fact that v_c is set according to the furthest UAV way-point from the laser source.

Fig. 6 shows that DMSCA and DMCS solutions tend to increase the power of the beacon source power transmission until it reaches the maximum value and maintains it within the data transmission window, then decreases to zero. This owes to the progression of the UAV's path where the initial way-points and the final way-points are far from the PDs, hence experiencing weak channels. EMSCA and EMCS solutions use the maximum beacon source power throughout the whole flight to shorten the flight as much as possible.

It is evident that the DMSCA and DMCS solutions push the laser source to use the maximum power throughout the whole flight duration, as shown in Fig. 7 and highlighted in the transition from (**P**3) to ($\tilde{\text{P}}$3). On the other hand, EMSCA and EMCS push the solution towards achieving the power budget constraint with equality by using the minimum feasible laser power. Hence, the laser radiated power profile is shaped by the UAV's distance from the laser source for the EMCS solution, while it is shaped by both the UAV-laser separation distance and the UAV's velocity for the EMSCA solution.

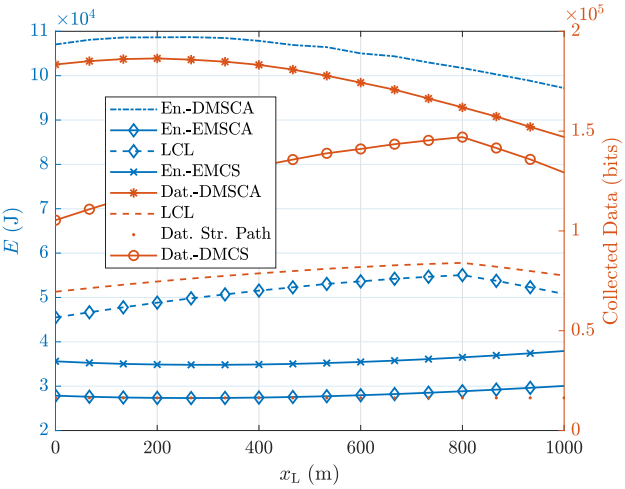

FIGURE 8. Laser location simulation.

B. PERFORMANCE EVALUATION

In the simulations presented in this section, we vary one of the system parameters and monitor its impact on the performance in terms of laser energy consumption and the total collected data for the proposed solutions. As changing the simulation parameters generally affects the collected data performance of the LCL solution (initial point for EMSCA and EMCS), we set $D_{\min}$ for each of the following simulations to 90% of the minimum value achieved by the LCL solutions associated with the study to ensure a fair comparison and feasibility of the problem.

By varying the laser location as shown in Fig. 8, it is observed that the collected data of the DMSCA solution exhibit unimodal behavior. The local maximum of this trend occurs around the laser source alignment with the center of the PDs' deployment region. The DMCS and the

initial solution show a similar collected data trend, albeit, at a different maximum location owing to constant speed restriction, which makes the optimal laser location different from the DMSCA case. On the other hand, the laser energy consumption of the EMSCA solution exhibits a unimodal behavior with a local minimum that mimics the UAV-laser source separation distance behavior. The EMCS solution follows a different trend in energy consumption compared to the EMSCA solution. This is due to the reduced impact of the relative PDs' deployment-laser location attributed to fixing the UAV's speed, which reduces the UAV maneuverability. Simulation results of changing the laser source y-coordinate while keeping the x-coordinate fixed produce similar conclusions and are not included for brevity.

In Fig. 9, the effect of the PD deployment is studied by altering the radius of the deployment circle. The performance of the collected data of all proposed solutions deteriorates as R_{s} increases. This is due to the deterioration of the wireless power links between the beacon source and the PDs as a result of increased pathloss. Similarly, the energy consumption increases with R_{s} as satisfying the same data collection requirement requires longer flight intervals.

In Fig. 10, we monitor the effect of the battery capacity of the power beacon source on the proposed solutions. It is observed that since the power beacon source is supplied with a larger-capacity battery, both the data maximization and the energy minimization solutions perform better. This is because of the system capability to support high-power transmission for longer intervals. Nevertheless, the performance enhancement saturates at a certain point when the system becomes able to offer the maximum radiated power for the entire flight duration. In this case, the maximum allowed radiated power by the power beacon source limits the system performance.

In Fig. 11 and Fig. 14,[4] the minimum aggregate and individual data requirements are increased, respectively, and the laser energy consumption is observed. It can be seen clearly that increasing $D_{\min}$ or $D_{\min}^{\mathrm{ind}}$ increases the laser energy consumption, as it requires the UAV's flight duration to be extended to collect the excess amount of data. In addition, it can be seen that the laser energy savings offered by optimization decreases as the data requirement increases and approaches the data amount provided by the initial solution.

Finally, the impact of the power beacon height on the system performance is studied and presented in Fig. 12. It can be seen that the average harvested data experiences a unimodal behavior that features a local maximum. The likelihood of line-of-sight (LoS) outweighs the increased propagation losses caused by greater distances when the beacon source is at a low altitude, resulting in this result. However, at higher altitudes, the LoS probability approaches saturation as the elevation angle approaches 90° while the propagation losses increase at the same pace. The energy performance exhibits a unimodal behavior as well, with a local minimum due to deterioration of channel gains between the power beacon source and the PD's for low and high heights due to low LoS probability and large path loss, respectively. Furthermore, it is clear that the optimal height power beacon deployment altitude depends on the altitude of the UAV as observed in Fig. 13. The performance gap between the DMSCA solution and the LCL solution stems from the constant speed and inconsideration of PDs layout features of the LCL solution. The straight path performs even worse due to the inconsideration of the power beacon source location.

In all simulations, the DMSCA solution showed superiority over the DMCS, which performs better than the initial solution, and all of them outperformed the straight-path solution. Similarly, the EMSCA solution outperforms all

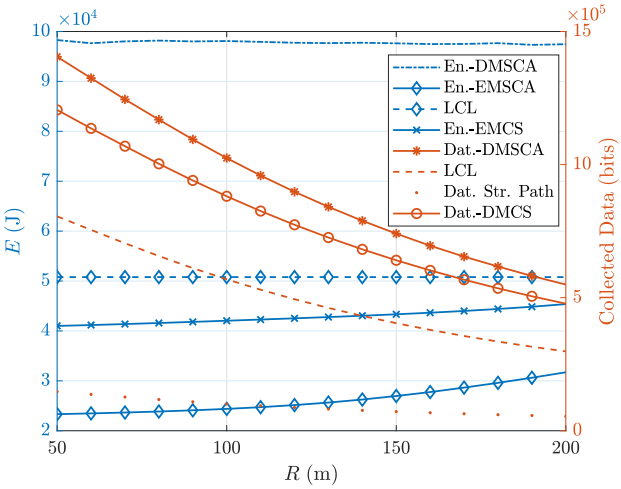

FIGURE 9. PDs deployment simulation.

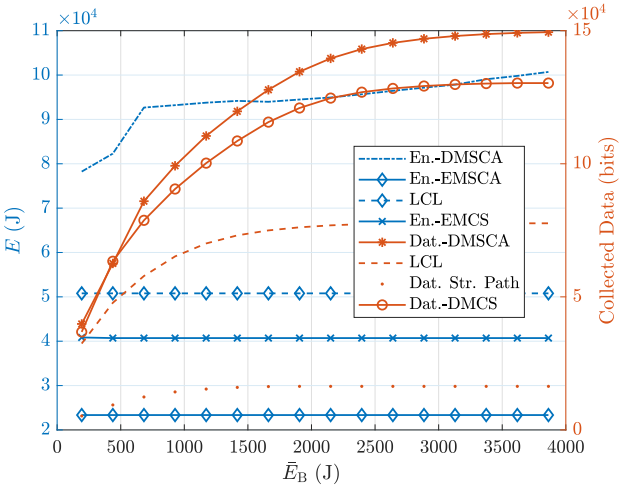

FIGURE 10. Power beacon battery capacity simulation.

[4]For the individual data requirement simulation, the PDs are deployed on two concentric circles centered around the power beacon source, having radii of 100 m and 200 m, each of which has nine PDs that are uniformly distributed angularly. $D_{\min}$ is kept negligible in this simulation, to make sure that C8 is active, and $D_{\min}^{\mathrm{ind}}$ is set as a fraction of the least individually achievable data transfer through the initial LCL solution.

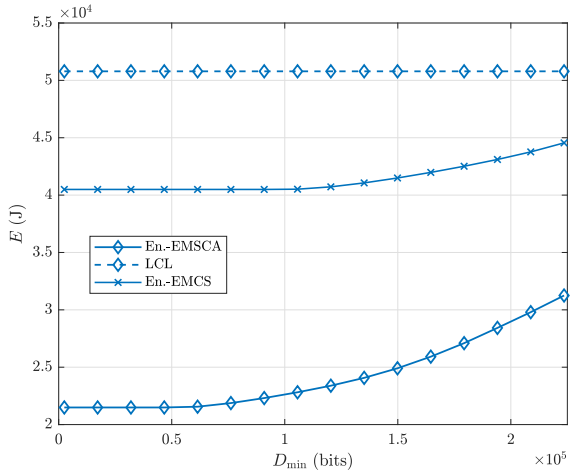

FIGURE 11. Minimum aggregate data requirement simulation.

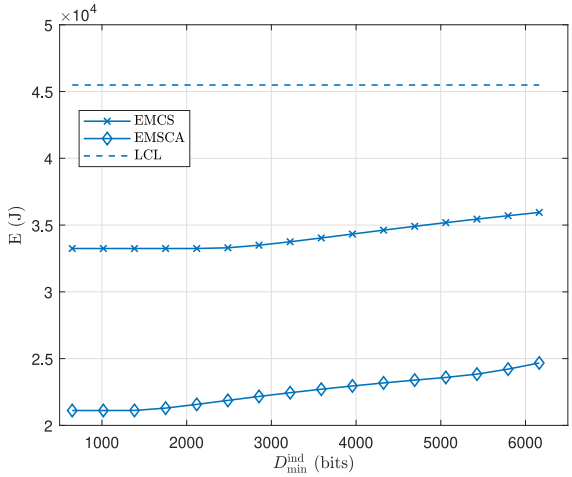

FIGURE 14. Minimum individual data requirement simulation.

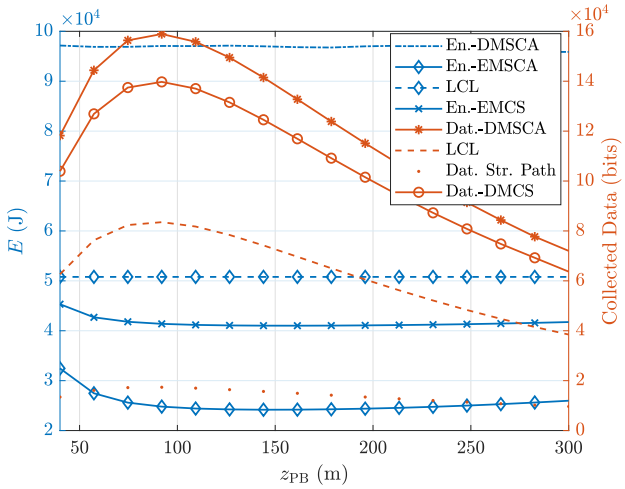

FIGURE 12. Average harvested data vs power beacon height.

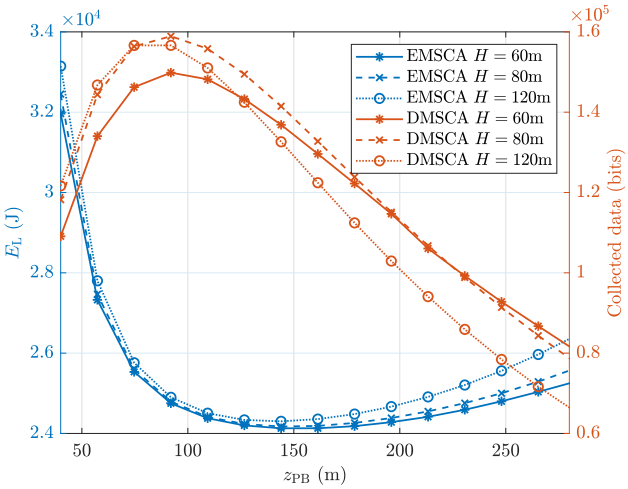

FIGURE 13. Average harvested data for different UAV heights.

other solutions, while the EMCS solution outperforms the initial solution. In addition, the trade-off between laser energy consumption and the collected data throughout the flight is clearly seen in the energy consumption gap between the DMSCA and the EMSCA solutions. Moreover, it is observed that the data collection performance improvement offered by DMSCA over DMCS fluctuates between 8% and 48% depending on the laser location, while DMSCA outperforms the LCL solution by 80% - 100%. On the energy consumption frontier, EMCS provides 29% laser energy reduction compared with the LCL solution, while the EMSCA solution provides 100% energy reduction for the majority of the simulation points.

VIII. CONCLUSION

In this paper, we considered a laser-powered fixed-wing UAV-aided data collection system serving an IoT field of passive devices via bistatic backscatter wireless links. We aimed at minimizing the laser source's overall energy consumption whilst guaranteeing a minimum amount of collected data from the passive devices. Towards this aim, we studied the UAV trajectory, and the radiated power profile of both the laser source and the power beacon source. Adopting path discretization, we solved the energy minimization problem and its associated feasibility problem via SCA over the joint set of variables. The conducted simulations highlighted the dependencies between the UAV path, dynamics and the system energy delivery behavior at both the laser station and the power beacon source. In particular, it was found that relaxing the UAV power budget enables the UAV to slow down over the IoT devices field and take sharper turns without violating the maximum acceleration magnitude constraint. Hence, the UAV can loop around the passive devices in tighter circles and collect the required amount of data in a shorter time.

APPENDIX A
ASYMPTOTIC APPROXIMATION OF PATH DISCRETIZED TIME INTERVALS PROOF

It can be noticed that for efficient sampling (guaranteeing that any two successive points are not more than Δ_M apart

with the least number of points), we need

$$N_{\mathrm{W}} = \left\lceil \frac{L}{\Delta_{\mathrm{M}}} \right\rceil \tag{26}$$

Hence,

$$\frac{L}{\Delta_{\mathrm{M}}} \leq N_{\mathrm{W}} < \frac{L}{\Delta_{\mathrm{M}}} + 1, \tag{27}$$

which is equivalent to

$$\frac{L}{N_{\mathrm{W}}} \leq \Delta < \frac{L}{N_{\mathrm{W}} - 1}. \tag{28}$$

Consequently, for fixed L, as N_{W} increases, the upper bound on Δ decreases. Now by adding the UAV's speed bounds $v_{\min} \leq v \leq v_{\max}$ and after some straightforward manipulations, we obtain

$$\begin{aligned} \frac{\|q[n] - q[n-1]\|}{v_{\max}} \leq \Delta t[n] \leq \frac{\|q[n] - q[n-1]\|}{v_{\min}} \\ \leq \frac{\Delta}{v_{\min}} < \frac{L}{(N_{\mathrm{W}} - 1) v_{\min}}, \end{aligned} \tag{29}$$

which leads to a decreasing bound on $|\Delta t[n] - \Delta t[n-1]|$ w.r.t. N_{W} as

$$|\Delta t[n] - \Delta t[m]| < \frac{L}{(N_{\mathrm{W}} - 1) v_{\min}}. \tag{30}$$

The previous inequality implies that $\Delta t[n]$ and $\Delta t[m]$ get closer as N_{W} increases.

APPENDIX B
SCA BOUNDS DERIVATIONS OF ($\tilde{\mathrm{P}}$1) AND (P3)

The subsequent theorems propose generic SCA-compatible bounds for the product of two positive convex functions and the product of a positive convex and a positive concave function, and are used heavily in the following SCA bound derivations.

Theorem 1: If $f(\boldsymbol{x}) \geq 0,\ \forall \boldsymbol{x} \in \mathcal{D}_1$, and $g(\boldsymbol{y}) \geq 0,\ \forall \boldsymbol{y} \in \mathcal{D}_2, f(.), g(.)$ are both convex over $\mathcal{D}_1, \mathcal{D}_2$, respectively, then

$$\begin{aligned} f(\boldsymbol{x})g(\boldsymbol{y}) \leq F(f,g) = \frac{1}{4}\Big(f_{\mathrm{s}}^2 + f_{\mathrm{d},o}^2 - 2f_{\mathrm{d},o} \\ \times \Big(I_1\Big(\tilde{f}_{\mathrm{s}} - f_{\mathrm{s}}\Big) + f(\boldsymbol{x}) - \tilde{g}(\boldsymbol{y})\Big)\Big), \forall (\boldsymbol{x},\boldsymbol{y}) \in \hat{\mathcal{D}}, (\boldsymbol{x_o},\boldsymbol{y_o}) \in \hat{\mathcal{D}}, \end{aligned}$$

s.t. $f_{\mathrm{s}} = f(\boldsymbol{x}) + g(\boldsymbol{y}), f_{\mathrm{d},o} = f(\boldsymbol{x}_o) - g(\boldsymbol{y}_o)$, $I_1 = 1$ if $f_{\mathrm{d},0} \geq 0$, $I_1 = 0$ o.w., $\tilde{\chi}(\boldsymbol{z}) = \chi(\boldsymbol{z}_o) + \nabla\chi^{\mathrm{T}}(\boldsymbol{z}_o)(\boldsymbol{z} - \boldsymbol{z}_o)$, $\hat{\mathcal{D}} = \mathcal{D}_1 \times \mathcal{D}_2$.

Proof:

$$\begin{aligned} 4f(\boldsymbol{x})g(\boldsymbol{y}) = f_{\mathrm{s}}^2 - f_{\mathrm{d}}^2 \overset{(a)}{\leq} f_{\mathrm{s}}^2 + f_{\mathrm{d},o}^2 - 2f_{\mathrm{d},o} f_{\mathrm{d}} \overset{(b)}{\leq} \\ f_{\mathrm{s}}^2 + f_{\mathrm{d},o}^2 - 2f_{\mathrm{d},o}(I_1(\tilde{f}(\boldsymbol{x}) - g(\boldsymbol{y})) + (1 - I_1)(f(\boldsymbol{x}) - \tilde{g}(\boldsymbol{y}))), \end{aligned}$$

where the convexity of f_{s}^2 holds as $(.)^2$ is a convex increasing function for positive argument. Hence, its composition with the convex f_{s} is convex. Particularly, (a) follows from lower bounding the $(.)^2$ function of the second term by its first order Taylor series (F.O.T) approximation. Similarly, (b) follows by decomposing f_{d} into $f_{\mathrm{d}} I_1$ and $f_{\mathrm{d}}(1 - I_1)$. Then, lower bounding the $f(\boldsymbol{x})$ term within the former and the $g(\boldsymbol{y})$ term the latter with their F.O.T approximations completes the proof. ■

Theorem 2: If $f(\boldsymbol{x}) \geq 0,\ \forall \boldsymbol{x} \in \mathcal{D}_1$, and $g(\boldsymbol{y}) \geq 0,\ \forall \boldsymbol{y} \in \mathcal{D}_2, f(.)$ is convex, $g(.)$ is concave over $\mathcal{D}_1, \mathcal{D}_2$, respectively, then

$$\begin{aligned} f(\boldsymbol{x})g(\boldsymbol{y}) \leq G(f,g) = \\ \frac{1}{4}\Big((f(\boldsymbol{x}) + \tilde{g}(\boldsymbol{y}))^2 + f_{\mathrm{d},o}^2 - 2f_{\mathrm{d},o}\Big(I_1\Big(\tilde{f}_{\mathrm{d}} - f_{\mathrm{d}}\Big) + f_{\mathrm{d}}\Big)\Big), \\ \forall (\boldsymbol{x},\boldsymbol{y}) \in \hat{\mathcal{D}}, (\boldsymbol{x_o},\boldsymbol{y_o}) \in \hat{\mathcal{D}}, f_{\mathrm{d}} = f(\boldsymbol{x}) - g(\boldsymbol{y}). \end{aligned}$$

Proof:

$$\begin{aligned} 4f(\boldsymbol{x})g(\boldsymbol{y}) \overset{(a)}{\leq} (f(\boldsymbol{x}) + \tilde{g}(\boldsymbol{y}))^2 + f_{\mathrm{d},o}^2 - 2f_{\mathrm{d},o} f_{\mathrm{d}} \\ \overset{(b)}{\leq} (f(\boldsymbol{x}) + \tilde{g}(\boldsymbol{y}))^2 + f_{\mathrm{d},o}^2 - 2f_{\mathrm{d},o}(I_1 \tilde{f}_{\mathrm{D}} + (1 - I_1) f_{\mathrm{D}}), \end{aligned}$$

where (a) follows from upper bounding $g(\boldsymbol{y})$ by its F.O.T. The convexity of $(f(\boldsymbol{x}) + \tilde{g}(\boldsymbol{y}))^2$ follows from the convexity and positiveness of the $(.)^2$ argument. Likewise, (b) follows by decomposing f_{D} as in the proof of Theorem 1, and lower bounding the convex f_{D} associated with I_1 by its F.O.T approximation. ■

A. AGGREGATE DATA SCA-COMPATIBLE LOWER BOUND DERIVATION

We first derive a lower bound for $\bar{D}_{\mathrm{LB},i}[n]$, presented in (18), by applying [46, Lemma 2] to get $(\bar{D}^{(1)}_{\mathrm{LB},i}[n])$. Next, through [46, Lemma 3], a lower bound on the latter term is obtained. Therefore, it follows: $\bar{D}_{\mathrm{LB},i}[n] \geq \bar{D}^{(1)}_{\mathrm{LB},i}[n] \geq \bar{D}^{(2)}_{\mathrm{LB},i}[n]$, with $\bar{D}^{(2)}_{\mathrm{LB},i}[n]$ expressed as

$$\bar{D}^{(2)}_{\mathrm{LB},i}[n] = P^{\mathrm{B}}_{\mathrm{L},i}\Big(T_i[n] - \hat{\Psi}_i[n]\Delta q^{\mathrm{u}}_{\mathrm{s}_i}[n]^2 - \hat{\Phi}_i[n] e^{\Delta\tilde{q}^{\mathrm{U}}_{\mathrm{s}_i}[n]}\Big), \tag{31}$$

$$T_i[n] = \hat{\bar{D}}^{\mathrm{L}}_i[n] + \hat{\Phi}_i[n]\Big(\hat{X}_i[n] - 1\Big) + \hat{\Psi}_i[n]\Delta q^{\mathrm{u}}_{\mathrm{s}_i,o}[n]^2, \tag{32}$$

$$\hat{\bar{D}}^{\mathrm{L}}_i[n] = \Delta t[n] P_{\mathrm{L}}\Big(\hat{\theta}^{\mathrm{U}}_i[n]\Big) \ln\left(1 + \frac{\zeta_{i,\mathrm{L}} \tilde{p}_{\mathrm{B}}[n]}{d^{\alpha_{\mathrm{L}}}_{i,\mathrm{u}}[n] \Delta t[n]}\right), \tag{33}$$

$$\hat{\Phi}_i[n] = \Delta t[n] \frac{C_2}{\hat{X}^2_i[n]} \ln\left(1 + \frac{\zeta_{i,\mathrm{L}} \tilde{p}_{\mathrm{B}}[n]}{d^{\alpha_{\mathrm{L}}}_{i,\mathrm{u}}[n] \Delta t[n]}\right), \tag{34}$$

$$\hat{\Psi}_i[n] = \frac{\Delta t[n] P_{\mathrm{L}}\Big(\hat{\theta}^{\mathrm{U}}_i[n]\Big) \zeta_{i,\mathrm{L}} \tilde{p}_{\mathrm{B}}[n] \alpha_{\mathrm{L}}/2}{d^{\alpha_{\mathrm{L}}}_{i,\mathrm{u},o}[n]\Big(\Delta t_n d^{\alpha_{\mathrm{L}}}_{i,\mathrm{u},o}[n] + \zeta_{i,\mathrm{L}} \tilde{p}_{\mathrm{B}}[n]\Big)}, \tag{35}$$

$$\hat{X}_i[n] = 1 + \exp\Big(-(B_1 + B_2 \hat{\theta}_i[n])\Big), \tag{36}$$

$$\begin{aligned} d_{i,\mathrm{u},o} &= \sqrt{\Delta q^{\mathrm{u}}_{\mathrm{s}_i,o}{}^2[n] + H^2}, \\ \tau_i[n] &= B_1 + \frac{180}{\pi} B_2 \left(\tan^{-1}\left(\frac{H}{\Delta q^{\mathrm{u}}_{\mathrm{s}_i,o}[n]}\right) + \frac{H \Delta q^{\mathrm{u}}_{\mathrm{s}_i,o}[n]}{d^2_{i,\mathrm{u},o}}\right), \\ \Delta\tilde{q}^{\mathrm{u}}_{\mathrm{s}_i}[n] &= -\tau_i[n] + 180/\pi B_2 H d^{-2}_{i,\mathrm{u},o} \Delta q^{\mathrm{u}}_{\mathrm{s}_i}[n], \\ \hat{\theta}_i[n] &= \frac{180}{\pi} \tan^{-1}\big(H/\Delta q^{\mathrm{u}}_{\mathrm{s}_i,o}[n]\big), \end{aligned} \tag{37}$$

$$\Delta q^{\mathrm{u}}_{\mathrm{s}_i,\chi}[n] = \sqrt{\Big(q^{\mathrm{u}}_{\mathrm{x},\chi}[n] - q^{\mathrm{s}}_{\mathrm{x},i}\Big)^2 + \Big(q^{\mathrm{u}}_{\mathrm{y},\chi}[n] - q^{\mathrm{s}}_{\mathrm{y},i}\Big)^2}, \chi \in \{\{\}, o\}. \tag{38}$$

By inspecting $\bar{D}^{(2)}_{\mathrm{LB},i}[n]$, the concavity of $T_i[n]$ can be deduced from its composition of positive sum of three terms that are the perspective transform of concave functions in the

joint set of variables. The remaining two terms, $\hat{\phi}_i[n]$ and $\hat{\psi}_i[n]$, are concave in the optimization parameters as they are the perspective transform of concave functions, which can be easily shown. In addition, $\exp(\beta\|.\|_2)$ is a convex function for $\beta \geq 0$ as it is the composition of a convex increasing function with another convex function. Hence, by upper bounding the remaining two products of a positive convex function and a positive concave function, the SCA-compatible lower bound for $\bar{D}_{\mathrm{LB},i}[n]$ is given by

$$\tilde{D}_{\mathrm{LB},i}[n] = P^{\mathrm{B}}_{\mathrm{L},i}\Big(T_i[n] - G\Big(\Delta q^{\mathrm{u}}_{\mathrm{s}_i}[n]^2, \hat{\Psi}_i[n]\Big) - G\Big(e^{\Delta \tilde{q}^{\mathrm{u}}_{\mathrm{s}_i}[n]}, \hat{\Phi}_i[n]\Big)\Big). \quad (39)$$

B.PROPULSION POWER SCA-COMPATIBLE UPPER BOUND DERIVATION

In terms of constraints, the SCA-compatible version of the minimum speed constraint can be obtained by lower bounding $\|\boldsymbol{q}^{\mathrm{u}}[n]-\boldsymbol{q}^{\mathrm{u}}[n-1]\|_2$ with its F.O.T approximation, $\tilde{s}[n]$, expressed as

$$\tilde{s}[n] = \|\boldsymbol{\Delta q}^{\mathrm{u}}_o[n]\|_2 + \frac{\boldsymbol{\Delta q}^{\mathrm{u}}_o[n]^{\mathrm{T}}\big(\boldsymbol{\Delta q}^{\mathrm{u}}[n] - \boldsymbol{\Delta q}^{\mathrm{u}}_o[n]\big)}{\big\|\boldsymbol{\Delta q}^{\mathrm{u}}_o[n]\big\|_2},$$

where $\boldsymbol{\Delta q}^{\mathrm{u}}[n] = \boldsymbol{q}^{\mathrm{u}}[n] - \boldsymbol{q}^{\mathrm{u}}[n-1]$ and $\boldsymbol{\Delta q}^{\mathrm{u}}_o[n] = \boldsymbol{q}^{\mathrm{u}}_o[n] - \boldsymbol{q}^{\mathrm{u}}_o[n-1]$. Similarly, $\Delta t^2[n]$ can be lower bounded by $\Delta\tilde{t}[n]$ as follows:

$$\Delta\tilde{t}[n] = \Delta t^2_o[n] + 2\Delta t_o[n](\Delta t[n] - \Delta t_o[n]). \quad (40)$$

Note that the propulsion power, denoted by $p_{\mathrm{R}}[n]$, introduces a non-convex constraint as well. However, such a term can be upper bounded by applying Theorem 1 to (a) its first term and (b) to the upper bound of the second term obtained by lower bounding the denominator with $\tilde{s}[n]$[5] to get $p_{\mathrm{R}}[n] \leq \hat{p}_{\mathrm{R}}[n]$ expressed as

$$\hat{p}_{\mathrm{R}}[n] = F\Big(\|\boldsymbol{\Delta q}^{\mathrm{u}}[n]\|_2^3, \Delta t^{-3}[n]\Big) + F\Big(\Delta t[n], \tilde{s}^{-1}[n]\Big). \quad (41)$$

C.HARVESTED POWER SCA-COMPATIBLE LOWER BOUND DERIVATION

For the harvested power presuming maximum radiated laser power, $\hat{P}_{\mathrm{H}}[n]$, by inspecting (15) and (16), it can be deduced that $\hat{P}_{\mathrm{H}}[n]$ is a convex decreasing function in $d^{\mathrm{u}}_{\mathrm{L}}[n]$. This owes to its composition of a convex increasing function in the generated photocurrent, which is convex and decreasing in $d^{\mathrm{u}}_{\mathrm{L}}[n]$. Accordingly, $\hat{P}_{\mathrm{H}}[n]$ can be lower bounded as

$$\hat{P}_{\mathrm{H}}[n] \geq E_1[n] - E_2[n]\big(d^{\mathrm{u}}_{\mathrm{L}}[n] - d^{\mathrm{u}}_{\mathrm{L},o}[n]\big) \triangleq \tilde{P}_{\mathrm{H}}[n], \quad (42)$$

$$E_1[n] = 0.75\mathrm{V_t}x_o[n]\ln(1 + x_o[n]/\mathrm{I_o}), \quad (43)$$

$$x_o[n] = A_{\mathrm{PD}}R_{\mathrm{PD}}p^{\max}_{\mathrm{L}}[n]e^{-\alpha d^{\mathrm{u}}_{\mathrm{L},o}[n]}r^{-2}_{\mathrm{L},o}[n], \quad (44)$$

$$E_2[n] = 0.75v_{\mathrm{t}}\Delta\theta A_{\mathrm{PD}}R_{\mathrm{PD}}\left(\ln\left(1 + \frac{x_o[n]}{I_o}\right) - \frac{x_o[n]}{I_o + x_o[n]}\right) \times p^{\max}_{\mathrm{L}}[n]e^{-\alpha d^{\mathrm{u}}_{\mathrm{L},o}[n]}r^{-3}_{\mathrm{L},o}[n]\big(r_{\mathrm{L},o}[n] + 2\big), \quad (45)$$

where $d^{\mathrm{u}}_{\mathrm{L},o} = \|\boldsymbol{q}^{\mathrm{u}}_o[n] - \boldsymbol{q}_{\mathrm{L}}\|_2$, and $r_{\mathrm{L},o}[n] = \mathrm{D}_o + \Delta\theta d^{\mathrm{u}}_{\mathrm{L},o}$.

[5] $\tilde{s}[n]$ is guaranteed to be positive by the virtue of C2a'.

Now we derive the SCA-compatible lower bound on the harvested power, $P_{\mathrm{H}}[n]$, when $p_{\mathrm{L}}[n]$ is a variable. Exploiting the convexity of $P_{\mathrm{H}}[n]$ with respect to x and its positive monotonicity for positive arguments, $P_{\mathrm{H}}[n]$ can be lower bounded as

$$P_{\mathrm{H}}[n] \geq a_o[n] + b_o[n]p_{\mathrm{L}}[n]L_{\mathrm{D}}[n], \quad (46)$$

$$L_{\mathrm{D}}[n] = \frac{A_{\mathrm{PD}}R_{\mathrm{PD}}e^{-\alpha\|\boldsymbol{q}^{\mathrm{u}}[n]-\boldsymbol{q}_{\mathrm{L}}\|_2}}{\big(\mathrm{D}_o + \Delta\theta\|\boldsymbol{q}^{\mathrm{u}}[n] - \boldsymbol{q}_{\mathrm{L}}\|_2\big)^2}, \quad (47)$$

$$a_o[n] = 0.75\mathrm{V_t}\frac{A_{\mathrm{PD}}R_{\mathrm{PD}}p_{\mathrm{L},o}[n]e^{-\alpha\|\boldsymbol{q}^{\mathrm{u}}_o[n]-\boldsymbol{q}_{\mathrm{L}}\|_2}}{\big(\mathrm{D}_o + \Delta\theta\|\boldsymbol{q}^{\mathrm{u}}_o[n] - \boldsymbol{q}_{\mathrm{L}}\|_2\big)^2} \times \ln\left(1 + \frac{A_{\mathrm{PD}}R_{\mathrm{PD}}p_{\mathrm{L},o}[n]e^{-\alpha\|\boldsymbol{q}^{\mathrm{u}}_o[n]-\boldsymbol{q}_{\mathrm{L}}\|_2}}{\mathrm{I}_o\big(\mathrm{D}_o + \Delta\theta\|\boldsymbol{q}^{\mathrm{u}}_o[n] - \boldsymbol{q}_{\mathrm{L}}\|_2\big)^2}\right) - b_o[n]\frac{A_{\mathrm{PD}}R_{\mathrm{PD}}p_{\mathrm{L},o}[n]e^{-\alpha\|\boldsymbol{q}^{\mathrm{u}}_o[n]-\boldsymbol{q}_{\mathrm{L}}\|_2}}{\big(\mathrm{D}_o + \Delta\theta\|\boldsymbol{q}^{\mathrm{u}}_o[n] - \boldsymbol{q}_{\mathrm{L}}\|_2\big)^2}, \quad (48)$$

$$b_o[n] = 0.75\mathrm{V_t}\left(\ln\left(1 + \frac{A_{\mathrm{PD}}R_{\mathrm{PD}}p_{\mathrm{L},o}[n]e^{-\alpha\|\boldsymbol{q}^{\mathrm{u}}_o[n]-\boldsymbol{q}_{\mathrm{L}}\|_2}}{\mathrm{I}_o\big(\mathrm{D}_o + \Delta\theta\|\boldsymbol{q}^{\mathrm{u}}_o[n] - \boldsymbol{q}_{\mathrm{L}}\|_2\big)^2}\right) + \frac{1}{1 + \frac{A_{\mathrm{PD}}R_{\mathrm{PD}}p_{\mathrm{L},o}[n]e^{-\alpha\|\boldsymbol{q}^{\mathrm{u}}_o[n]-\boldsymbol{q}_{\mathrm{L}}\|_2}}{\mathrm{I}_o\big(\mathrm{D}_o + \Delta\theta\|\boldsymbol{q}^{\mathrm{u}}_o[n] - \boldsymbol{q}_{\mathrm{L}}\|_2\big)^2}}\right). \quad (49)$$

Since $L_{\mathrm{D}}[n]$ is convex in $\|\boldsymbol{q}^{\mathrm{u}}[n] - \boldsymbol{q}_{\mathrm{L}}\|_2$, we lower bound it using its F.O.T approximation as

$$L_{\mathrm{D}}[n] \geq c_o[n] - d_o[n]\|\boldsymbol{q}^{\mathrm{u}}[n] - \boldsymbol{q}_{\mathrm{L}}\|_2,$$
$$c_o[n] = \frac{A_{\mathrm{PD}}R_{\mathrm{PD}}p_{\mathrm{L},o}[n]e^{-\alpha\|\boldsymbol{q}^{\mathrm{u}}_o[n]-\boldsymbol{q}_{\mathrm{L}}\|_2}}{\big(\mathrm{D}_o + \Delta\theta\|\boldsymbol{q}^{\mathrm{u}}_o[n] - \boldsymbol{q}_{\mathrm{L}}\|_2\big)^2} + d_o[n]\,\|\boldsymbol{q}^{\mathrm{u}}_o[n] - \boldsymbol{q}_{\mathrm{L}}\|_2,$$
$$d_o[n] = \frac{\alpha\big(\mathrm{D}_o + \Delta\theta\|\boldsymbol{q}^{\mathrm{u}}_o[n] - \boldsymbol{q}_{\mathrm{L}}\|_2\big) + 2\Delta\theta}{\big(\mathrm{D}_o + \Delta\theta\|\boldsymbol{q}^{\mathrm{u}}_o[n] - \boldsymbol{q}_{\mathrm{L}}\|_2\big)^3} \times A_{\mathrm{PD}}R_{\mathrm{PD}}p_{\mathrm{L},o}[n]e^{-\alpha\|\boldsymbol{q}^{\mathrm{u}}_o[n]-\boldsymbol{q}_{\mathrm{L}}\|_2}. \quad (50)$$

Hence, $P_{\mathrm{H}}[n]$ can be further lower bounded as

$$P_{\mathrm{H}}[n] \geq a_o[n] + b_o[n]p_{\mathrm{L}}[n]\big(c_o[n] - d_o[n]\|\boldsymbol{q}^{\mathrm{u}}[n] - \boldsymbol{q}_{\mathrm{L}}\|_2\big). \quad (51)$$

The remaining sole source of non-convexity in the previous SCA compatible lower bound is the product term $p_{\mathrm{L}}[n]\|\boldsymbol{q}^{\mathrm{u}}[n] - \boldsymbol{q}_{\mathrm{L}}\|_2$, hence, we upper bound it using Theorem 1 as

$$p_{\mathrm{L}}[n]\|\boldsymbol{q}^{\mathrm{u}}[n] - \boldsymbol{q}_{\mathrm{L}}\|_2 \leq f^{\mathrm{UB}}_n[n] = \frac{1}{4}\Bigg(\big(p_{\mathrm{L}}[n] + \|\boldsymbol{q}^{\mathrm{u}}[n] - \boldsymbol{q}_{\mathrm{L}}\|_2\big)^2 + \big(p_{\mathrm{L},o}[n] - \|\boldsymbol{q}^{\mathrm{u}}_o[n] - \boldsymbol{q}_{\mathrm{L}}\|_2\big)^2 - 2\big(p_{\mathrm{L},o}[n] - \|\boldsymbol{q}^{\mathrm{u}}_o[n] - \boldsymbol{q}_{\mathrm{L}}\|_2\big)\Bigg(p_{\mathrm{L}}[n] - I_5\|\boldsymbol{q}^{\mathrm{u}}_n - \boldsymbol{q}_{\mathrm{L}}\|_2 + I_6 \times\left(\|\boldsymbol{q}^{\mathrm{u}}[n] - \boldsymbol{q}_{\mathrm{L}}\|_2 + \frac{\big(\boldsymbol{q}^{\mathrm{u}}_o[n] - \boldsymbol{q}_{\mathrm{L}}\big)^{\mathrm{T}}\big(\boldsymbol{q}^{\mathrm{u}}_n - \boldsymbol{q}^{\mathrm{u}}_o[n]\big)}{\|\boldsymbol{q}^{\mathrm{u}}_o[n] - \boldsymbol{q}_{\mathrm{L}}\|_2}\right)\Bigg)\Bigg), \quad (52)$$

where $I_5 = \mathcal{I}(p_{\mathrm{L},o}[n] \geq ||\boldsymbol{q}_o^{\mathrm{u}}[n] - \boldsymbol{q}_{\mathrm{L}}||_2)$ and $I_6 = 1 - I_5$. Finally, an SCA compatible lower bound for $P_{\mathrm{H}}[n]$ is given as

$$P_{\mathrm{H}}[n] \geq \tilde{P}_{\mathrm{H},2}[n] = a_o[n] + b_o[n]c_o[n]p_{\mathrm{L}}[n] - b_o[n]d_o[n]f_n^{\mathrm{UB}}[n]. \quad (53)$$

REFERENCES

[1] E. Koyuncu, R. Khodabakhsh, N. Surya, and H. Seferoglu, "Deployment and trajectory optimization of UAVs: A quantization theory approach," *IEEE Trans. Wireless Commun.*, vol. 17, no. 12, pp. 8531–8546, Dec. 2018.

[2] J. Guo, P. Walk, and H. Jafarkhani, "Optimal deployments of UAVs with directional antennas for a power-efficient coverage," *IEEE Trans. Commun.*, vol. 68, no. 8, pp. 5159–5174, Aug. 2020.

[3] C. Diaz-Vilor, A. Lozano, and H. Jafarkhani, "Cell-free UAV networks: Asymptotic analysis and deployment optimization," *IEEE Trans. Wireless Commun.*, vol. 22, no. 5, pp. 3055–3070, May 2023.

[4] C. Diaz-Vilor, A. Lozano, and H. Jafarkhani, "Cell-free UAV networks with wireless fronthaul: Analysis and optimization," *IEEE Trans. Wireless Commun.*, early access, Jul. 18, 2023, doi: 10.1109/TWC.2023.3294908.

[5] R. Abdelfatah, N. Alshaer, and T. Ismail, "A review on pointing, acquisition, and tracking approaches in UAV-based FSO communication systems," *Opt. Quant. Electron.*, vol. 54, no. 9, p. 571, 2022.

[6] Y. Kaymak, R. Rojas-Cessa, J. Feng, N. Ansari, M. Zhou, and T. Zhang, "A survey on acquisition, tracking, and pointing mechanisms for mobile free-space optical communications," *IEEE Commun. Surveys Tuts.*, vol. 20, no. 2, pp. 1104–1123, 2nd Quart., 2018.

[7] M.-A. Lahmeri, M. A. Kishk, and M.-S. Alouini, "Charging techniques for UAV-assisted data collection: Is laser power beaming the answer?" *IEEE Commun. Mag.*, vol. 60, no. 5, pp. 50–56, May 2022.

[8] P. D. Diamantoulakis, K. N. Pappi, Z. Ma, X. Lei, P. C. Sofotasios, and G. K. Karagiannidis, "Airborne radio access networks with simultaneous lightwave information and power transfer (SLIPT)," in *Proc. IEEE Global Telecommun. Conf.*, 2018, pp. 1–6.

[9] A. M. Abdelhady, O. Amin, M.-S. Alouini, and B. Shihada, "Revolutionizing optical wireless communications via smart optics," *IEEE Open J. Commun. Soc.*, vol. 3, pp. 654–669, 2022.

[10] W. Liu, L. Zhang, and N. Ansari, "Laser charging enabled DBS placement for downlink communications," *IEEE Trans. Netw. Sci. Eng.*, vol. 8, no. 4, pp. 3009–3018, Oct.–Dec. 2021.

[11] J. Ouyang, Y. Che, J. Xu, and K. Wu, "Throughput maximization for laser-powered UAV wireless communication systems," in *Proc. IEEE Int. Conf. Commun. Workshops*, 2018, pp. 1–6.

[12] M.-M. Zhao, Q. Shi, and M.-J. Zhao, "Efficiency maximization for UAV-enabled mobile relaying systems with laser charging," *IEEE Trans. Wireless Commun.*, vol. 19, no. 5, pp. 3257–3272, 2020.

[13] M.-A. Lahmeri, M. A. Kishk, and M.-S. Alouini, "Laser-powered UAVs for wireless communication coverage: A large-scale deployment strategy," *IEEE Trans. Wireless Commun.*, vol. 22, no. 1, pp. 518–533, Jan. 2023.

[14] Z. Cheng, Z. Gao, M. Liwang, L. Huang, X. Du, and M. Guizani, "Intelligent task offloading and energy allocation in the UAV-aided mobile edge-cloud continuum," *IEEE Netw.*, vol. 35, no. 5, pp. 42–49, Sep./Oct. 2021.

[15] M. S. Bashir and M.-S. Alouini, "Energy optimization of a laser-powered hovering-UAV relay in optical wireless backhaul," *IEEE Trans. Wireless Commun.*, vol. 22, no. 5, pp. 3216–3230, May 2023.

[16] A. Ranjha and G. Kaddoum, "URLLC-enabled by laser powered UAV relay: A quasi-optimal design of resource allocation, trajectory planning and energy harvesting," *IEEE Trans. Veh. Technol.*, vol. 71, no. 1, pp. 753–765, Jan. 2022.

[17] O. S. Oubbati, A. Lakas, and M. Guizani, "Multiagent deep reinforcement learning for wireless-powered UAV networks," *IEEE Internet Things J.*, vol. 9, no. 17, pp. 16044–16059, Sep. 2022.

[18] Y. Du, K. Wang, K. Yang, and G. Zhang, "Trajectory design of laser-powered multi-drone enabled data collection system for smart cities," in *Proc. IEEE Global Telecommun. Conf.*, 2019, pp. 1–6.

[19] C. Abou-Rjeily, G. Kaddoum, and G. K. Karagiannidis, "Ground-to-air FSO communications: When high data rate communication meets efficient energy harvesting with simple designs," *Opt. Exp.*, vol. 27, no. 23, pp. 34079–34092, 2019.

[20] W. Jaafar and H. Yanikomeroglu, "Dynamics of laser-charged UAVs: A battery perspective," *IEEE Internet Things J.*, vol. 8, no. 13, pp. 10573–10582, Jul. 2021.

[21] S. Yang, Y. Deng, X. Tang, Y. Ding, and J. Zhou, "Energy efficiency optimization for UAV-assisted backscatter communications," *IEEE Commun. Lett.*, vol. 23, no. 11, pp. 2041–2045, Nov. 2019.

[22] G. Yang, R. Dai, and Y.-C. Liang, "Energy-efficient UAV backscatter communication with joint trajectory design and resource optimization," *IEEE Trans. Wireless Commun.*, vol. 20, no. 2, pp. 926–941, Feb. 2021.

[23] H. Yang, Y. Ye, X. Chu, and S. Sun, "Energy efficiency maximization for UAV-enabled hybrid backscatter-harvest-then-transmit communications," *IEEE Trans. Wireless Commun.*, vol. 21, no. 5, pp. 2876–2891, May 2022.

[24] Y. Nie, J. Zhao, J. Liu, J. Jiang, and R. Ding, "Energy-efficient UAV trajectory design for backscatter communication: A deep reinforcement learning approach," *China Commun.*, vol. 17, no. 10, pp. 129–141, Oct. 2020.

[25] R. Han, L. Bai, Y. Wen, J. Liu, J. Choi, and W. Zhang, "UAV-aided backscatter communications: Performance analysis and trajectory optimization," *IEEE J. Sel. Areas Commun.*, vol. 39, no. 10, pp. 3129–3143, Oct. 2021.

[26] X. Zhang, W. Luo, Y. Shen, and S. Wang, "Average AoI minimization in UAV-assisted IoT backscatter communication systems with updated information," in *Proc. IEEE SmartWorld, Ubiquitous Intell. Comput., Adv. Trusted Comput., Scalable Comput. Commun., Internet People Smart City Innov. (SmartWorld/SCALCOM/UIC/ATC/IOP/SCI)*, 2021, pp. 123–130.

[27] Z. Wang, D. Hong, Z. Fan, X. Wan, Y. Xu, and B. Duo, "Resource allocation for UAV-assisted backscatter communication," *EURASIP J. Wireless Commun. Netw.*, vol. 2022, p. 104, Oct. 2022.

[28] S.-H. Yeh, Y.-S. Wang, T. D. P. Perera, Y.-W. P. Hong, and D. N. K. Jayakody, "UAV trajectory optimization for data-gathering from backscattering sensor networks," in *Proc. IEEE Int. Conf. Commun.*, 2020, pp. 1–6.

[29] H. D. Tran, S. Chatzinotas, and B. Ottersten, "Throughput maximization for backscatter-and cache-assisted wireless powered UAV technology," *IEEE Trans. Veh. Technol.*, vol. 71, no. 5, pp. 5187–5202, May 2022.

[30] A. Farajzadeh, O. Ercetin, and H. Yanikomeroglu, "UAV data collection over NOMA backscatter networks: UAV altitude and trajectory optimization," in *Proc. IEEE Int. Conf. Commun*, 2019, pp. 1–7.

[31] J. Hu, X. Cai, and K. Yang, "Joint trajectory and scheduling design for UAV aided secure backscatter communications," *IEEE Wireless Commun. Lett.*, vol. 9, no. 12, pp. 2168–2172, Dec. 2020.

[32] M. Hua, L. Yang, C. Li, Q. Wu, and A. L. Swindlehurst, "Throughput maximization for UAV-aided backscatter communication networks," *IEEE Trans. Commun.*, vol. 68, no. 2, pp. 1254–1270, Feb. 2020.

[33] Y.-C. Liang, Q. Zhang, J. Wang, R. Long, H. Zhou, and G. Yang, "Backscatter communication assisted by reconfigurable intelligent surfaces," *Proc. IEEE*, vol. 110, no. 9, pp. 1339–1357, Sep. 2022.

[34] C. Pan et al., "An overview of signal processing techniques for RIS/IRS-aided wireless systems," *IEEE J. Sel. Top. Signal Process.*, vol. 16, no. 5, pp. 883–917, Aug. 2022.

[35] Z. Zhang et al., "Active RIS vs. passive RIS: Which will prevail in 6G?" *IEEE Trans. Commun.*, vol. 71, no. 3, pp. 1707–1725, Mar. 2023.

[36] C. You and R. Zhang, "Wireless communication aided by intelligent reflecting surface: Active or passive?" *IEEE Wireless Commun. Lett.*, vol. 10, no. 12, pp. 2659–2663, Dec. 2021.

[37] M. Z. Hassan, M. J. Hossain, J. Cheng, and V. C. M. Leung, "Statistical-QoS guarantee for IoT network driven by laser-powered UAV relay and RF backscatter communications," *IEEE Trans. Green Commun. Netw.*, vol. 5, no. 1, pp. 406–425, Mar. 2021.

[38] S. Chandrasekharan et al., "Designing and implementing future aerial communication networks," *IEEE Commun. Mag.*, vol. 54, no. 5, pp. 26–34, May 2016.

[39] J. D. Griffin and G. D. Durgin, "Complete link budgets for backscatter-radio and RFID systems," *IEEE Antennas Propag. Mag.*, vol. 51, no. 2, pp. 11–25, Apr. 2009.
[40] N. Van Huynh, D. T. Hoang, X. Lu, D. Niyato, and P. Wang, *IEEE Commun. Surveys Tuts.*, vol. 20, no. 4, pp. 2889–2922, 4th Quart., 2018.
[41] Y. Zeng, J. Xu, and R. Zhang, "Energy minimization for wireless communication with rotary-wing UAV," *IEEE Trans. Wireless Commun.*, vol. 18, no. 4, pp. 2329–2345, Apr. 2019.
[42] C. M. Lambert, "Dynamics modeling and conceptual design of a multi-tethered aerostat system," M.S. thesis, Dept. Mech. Eng., Univ. Victoria, Victoria, BC, Canada, 2002.
[43] S. S. Muhammad, P. Kohldorfer, and E. Leitgeb, "Channel modeling for terrestrial free space optical links," in *Proc. 7th Int. Conf. Transparent Opt. Netw.*, vol. 1, 2005, pp. 407–410.
[44] M. Ijaz, Z. Ghassemlooy, J. Pesek, O. Fiser, H. Le Minh, and E. Bentley, "Modeling of fog and smoke attenuation in free space optical communications link under controlled laboratory conditions," *J. Lightw. Technol.*, vol. 31, no. 11, pp. 1720–1726, Jun. 1, 2013.
[45] H. Kaushal, V. K. Jain, and S. Kar, *Free Space Optical Communication* (Optical Networks). New Delhi, India: Springer, 2017.
[46] C. You and R. Zhang, "Hybrid offline-online design for UAV-enabled data harvesting in probabilistic LoS channels," *IEEE Trans. Wireless Commun.*, vol. 19, no. 6, pp. 3753–3768, Jun. 2020.
[47] A. Al-Hourani, S. Kandeepan, and S. Lardner, "Optimal LAP altitude for maximum coverage," *IEEE Wireless Commun. Lett.*, vol. 3, no. 6, pp. 569–572, Dec. 2014.
[48] E. Lorenzo, *Solar Electricity: Engineering of Photovoltaic Systems*. Sterling, VA, USA: Earthscan/James & James, 1994.
[49] D. Killinger, "Free space optics for laser communication through the air," *Opt. Photon. news*, vol. 13, no. 10, pp. 36–42, 2002.
[50] J. Zhang, Y. Zeng, and R. Zhang, "Receding horizon optimization for energy-efficient UAV communication," *IEEE Wireless Commun. Lett.*, vol. 9, no. 4, pp. 490–494, Apr. 2020.
[51] Y. Zeng and R. Zhang, "Energy-efficient UAV communication with trajectory optimization," *IEEE Trans. Wireless Commun.*, vol. 16, no. 6, pp. 3747–3760, Jun. 2017.
[52] H. D. Young, *University Physics With Modern Physics*, 13th ed. Reading, MA, USA: Addison-Wesley, 2011.

AMR M. ABDELHADY (Member, IEEE) received the B.Sc. degree (Hons.) in communications and computer engineering from Cairo University, Giza, Egypt, in 2012, and the M.Sc. and Ph.D. degrees in electrical engineering from the King Abdullah University of Science and Technology, Thuwal, Makkah, Saudi Arabia, in 2016, and 2021, respectively, where he is currently a Postdoctoral Fellow. His general research interests lie in communications theory and signal processing for communications with special emphasis on non-terrestrial networks and optical wireless communications systems. Specific research areas include UAV communications, visible light communications, green communications, energy harvesting, and reconfigurable intelligent surfaces.

ABDULKADIR CELIK (Senior Member, IEEE) received the first M.S. degree in electrical engineering in 2013, the second M.S. degree in computer engineering in 2015, and the Ph.D. degree in electrical engineering and computer engineering from Iowa State University, Ames, IA, USA, in 2016. He was a Postdoctoral Fellow with the King Abdullah University of Science and Technology, Thuwal, Saudi Arabia, from 2016 to 2020, where he is currently a Senior Research Scientist with the Communications and Computing Systems Laboratory. His research interests are in the broad areas of next-generation wireless communication systems and networks. He currently serves as an Editor for IEEE COMMUNICATIONS LETTERS, IEEE WIRELESS COMMUNICATION LETTERS, and *Frontiers in Communications and Networks*. Dr. Celik is the recipient of the IEEE Communications Society's 2023 Outstanding Young Researcher Award for Europe, Middle East, and Africa Region.

CARLES DIAZ-VILOR (Student Member, IEEE) received the B.S. and M.S. degrees from the Polytechnic University of Catalonia, Barcelona, Spain, in 2017 and 2019, respectively. He is currently pursuing the Ph.D. in electrical engineering with the University of California at Irvine, Irvine, CA, USA. His current research interests are wireless communications and signal processing with an emphasis on UAV and sensor networks.

HAMID JAFARKHANI (Fellow, IEEE) is a Chancellor's Professor with the Department of Electrical Engineering and Computer Science, University of California at Irvine, Irvine, where he is also the Director of the Center for Pervasive Communications and Computing, the former Director of Networked Systems Program, and the Conexant-Broadcom Endowed Chair. He was a Visiting Scholar with Harvard University in 2015 and a Visiting Professor with the California Institute of Technology in 2018. He was the 2020–2022 elected Faculty Chair of the UCI School of Engineering. He is the author of the book *Space-Time Coding: Theory and Practice*.

Dr. Jafarkhani's awards are the NSF Career Award, the UCI Distinguished Mid-Career Faculty Award for Research, the School of Engineering Excellence in Research Senior Career Award, the IEEE Marconi Prize Paper Award in Wireless Communications, the IEEE Communications Society Award for Advances in Communication, the IEEE Wireless Communications Technical Committee Recognition Award, the IEEE Signal Processing and Computing for Communications Technical Recognition Award, couple of conference best paper awards, and the IEEE Eric E. Sumner Award. He is listed as an ISI highly cited researcher. According to the Thomson Scientific, he is one of the top 10 most-cited researchers in the field of "computer science" from 1997 to 2007. He is the 2017 Innovation Hall of Fame Inductee at the University of Maryland's School of Engineering. He was an Associate Editor for the IEEE COMMUNICATIONS LETTERS from 2001 to 2005, an Editor for the IEEE TRANSACTIONS ON WIRELESS COMMUNICATIONS from 2002 to 2007, an Editor for the IEEE TRANSACTIONS ON COMMUNICATIONS from 2005 to 2007, an Area Editor for the IEEE TRANSACTIONS ON WIRELESS COMMUNICATIONS from 2007 to 2012, and a Steering Committee Member of the IEEE TRANSACTIONS ON WIRELESS COMMUNICATIONS from 2013 to 2016. He was the General Chair of the 2015 IEEE Communication Theory Workshop and the General Co-Chair of the 2018 IEEE Global Conference on Signal and Information Processing. He was an IEEE ComSoc Distinguished lecturer. He is a Fellow of AAAS.

AHMED M. ELTAWIL (Senior Member, IEEE) received the B.Sc. and M.Sc. degrees (Hons.) from Cairo University, Giza, Egypt, in 1997 and 1999, respectively, and the Ph.D. degree from the University of California at Los Angeles, Los Angeles, in 2003. He is currently a Professor of Electrical and Computer Engineering with the King Abdullah University of Science and Technology (KAUST), where he joined the Computer, Electrical and Mathematical Science and Engineering Division in 2019. Prior to that, he has been with the Electrical Engineering and Computer Science Department, University of California at Irvine, Irvine, since 2005. At KAUST, he is the Founder and the Director of the Communication and Computing Systems Laboratory. His current research interests include the general area of smart and connected systems with an emphasis on mobile systems. He received several awards, including the NSF CAREER Grant supporting his research in low power computing and communication systems. He received two United States Congressional certificates recognizing his contributions to research and innovation. In 2021, he was selected as the "Innovator of the Year" by the Henry Samueli School of Engineering, University of California, Irvine. He has been on the technical program committees and steering committees for numerous workshops, symposia, and conferences in the areas of low power computing and wireless communication system design. He is a Senior Member of the National Academy of Inventors, USA.